Review

Valley manipulation in monolayer transition metal dichalcogenides and their hybrid systems: status and challenges

Siwen Zhao[1,2], Xiaoxi Li[3,4] ⓘ **, Baojuan Dong[5,6], Huide Wang[1], Hanwen Wang[3,4]** ⓘ **, Yupeng Zhang[1], Zheng Han[5,6,*]** ⓘ **and Han Zhang[1,*]**

[1] Key Laboratory of Optoelectronic Devices and Systems of Ministry of Education and Guangdong Province, International Collaborative Laboratory of 2D Materials for Optoelectronics Science and Technology of Ministry of Education, Institute of Microscale Optoelectronics, Shenzhen University, Shenzhen 518060, People's Republic of China
[2] College of Materials Science and Engineering, Shenzhen University, Shenzhen 518060, People's Republic of China
[3] Shenyang National Laboratory for Materials Science, Institute of Metal Research, Chinese Academy of Sciences, Shenyang, People's Republic of China
[4] School of Material Science and Engineering, University of Science and Technology of China, Hefei 230026, People's Republic of China
[5] State Key Laboratory of Quantum Optics and Quantum Optics Devices, Institute of Opto-Electronics, Shanxi University, Taiyuan 030006, People's Republic of China
[6] Collaborative Innovation Center of Extreme Optics, Shanxi University, Taiyuan 030006, People's Republic of China

E-mail: vitto.han@gmail.com and hzhang@szu.edu.cn

CrossMark

Abstract
Recently, the emerging conceptual valley-related devices have attracted much attention due to the progress on generating, controlling, and detecting the valley degree of freedom in the transition metal dichalcogenide (TMD) monolayers. In general, it is known that achieving valley degree of freedom with long valley lifetime is crucial in the implementation of valleytronic devices. Here, we provide a brief introduction of the basic understandings of valley degree of freedom. We as well review the recent experimental advancement in the modulation of valley degree of freedom. The strategies include optical/magnetic/electric field tuning, moiré patterns, plasmonic metasurface, defects and strain engineering. In addition, we summarize the corresponding mechanisms, which can help to obtain large degree of polarization and long valley lifetimes in monolayer TMDs. Based on these methods, two-dimensional valley-optoelectronic systems based on TMD heterostructures can be constructed, providing opportunities for such as the new paradigm in data processing and transmission. Challenges and perspectives on the development of valleytronics are highlighted as well.

Keywords: valleytronics, transition metal dichalcogenides (TMDs), optoelectronic devices, hybrid heterostructures

(Some figures may appear in colour only in the online journal)

---

1. Introduction

In certain crystals, in spite of spin and charge, electrons possess a valley degree of freedom. 'Valley' refers to energetically degenerate energy bands that hold non-equivalent local maxima for valence bands or minima for conduction bands. Since the valleys are often separated by a large crystal momentum, the intervalley scattering time (valley lifetime) of electrons can be very long in materials in the clean limit. Thanks to the possibly very long lifetime, valley degree of freedom is believed to be a totally new route of encoding information and may offer novel means for information storage as well as information processing, surpassing conventional charge- and spin-based applications. Moreover, valleytronic devices can be strongly coupled to photon spins, which often exhibit large valley polarization. It thus may lead to novel spin-valley devices in applications such as ultrafast optical manipulations. Some of the valleytronic devices can as well take the advantages of large Berry curvature to induce topological phenomena and the emerging experimental advancements.

The study of valley degree of freedom is not fresh. The first materials that demonstrated valley-related physics are traditional semiconductors including diamond, silicon, bismuth and group III–V semiconductors [1–5]. However, selectively initialize, manipulate, and readout the valley states of these materials remain exclusive due to the weak coupling between valley index and an external field. More recently, two dimensional (2D) layered materials such as graphene and group VI layered transition metal dichalcogenides (TMDs)-MX_2 (M: Mo, W and X: S, Se) have attracted wide attention because they may intrinsically possess or be modulated to exploit valley polarization [6–8]. In particular, in systems that lack inversion symmetry such as monolayer (ML) TMDs, both the values of Berry curvature and the orbital magnetic moments at $\pm K$ points are opposite, giving rise to two non-degenerating valleys. Because of the strong spin–orbit coupling and inversion symmetry broken in ML-TMDs, the spin-valley locked physics and chiral optical selection rules are observed [9–11]. Under the excitation of circularly polarized light, carriers can be selectively pumped into a corresponding valley with a particular pseudo-spin [8, 12–16]. In addition, external electric and magnetic fields can also manipulate the valley pseudo-spin because they are coupled to the valley contrasted Berry curvatures and orbital magnetic moments [17–19]. Therefore, ML TMDs are considered as outstanding platforms for exploring valley-related physics and valleytronic applications.

However, low degree of valley polarization and short intervalley scattering times (valley lifetimes) in ML-TMDs at room temperature hinder the usage of valley pseudospin in on-chip integrated devices. One way to overcome the obstacle is lifting the initial degree of circular polarization by introducing external fields because the applied non-resonant optical excitations and external magnetic fields could break valley degeneracy by optical Stark effect and Zeeman effects, respectively. Besides, intervalley scattering could also be effectively suppressed by electric field or electrostatic doping, which contributes to long valley lifetimes and large degree of valley polarization [20–23].

Furthermore, valley polarization could also be tailored by modulating exciton lifetimes because the degree of valley polarization is inversely proportional to exciton lifetimes. Exploiting electron-phonon interactions and charge-transfer processes can open available avenues towards tuning exciton lifetimes and thus degree of valley polarization [24, 25]. It is noteworthy that defects in ML-TMDs have complicated influence on valley polarization because they not only can modify the initial degree of circular polarization but also tailor the exciton lifetimes and intervalley scattering time [26, 27].

Additionally, recent developments of hybrid heterostructures based on TMDs exhibit the capability to effectively engineer valley polarization. For example, the interfacial magnetic exchange field from ferromagnetic (FM) substrates could tremendously enhance valley splitting in ML TMDs [28, 29]. The valley lifetimes of interlayer excitons (IX) in twisted heterobilayer TMDs can be increased to the order of μs [30, 31]. Combining plasmonic field and TMDs could increase valley polarization and spatially separate valley index [32, 33]. Therefore, it is essential to investigate different modulating methods and mechanisms for valley polarization, which may pave the way for future exploration of TMD-based room-temperature valleytronic devices.

Herein, we will give a brief introduction of valley degree of freedom in TMDs and summarize the various strategies and their corresponding mechanisms for engineering the valley degree of freedom. In the present review, we focus on strategies including optical pumping, external magnetic fields, electrostatic doping, defects engineering, strain, and interfacial effects in heterostructures based on FM substrates, plasmonic architectures and moiré patterns (figure 1). Then recent progress on valley manipulation in the valley-photonic and optoelectronic devices is highlighted. We close with the challenges and opportunities for the venture of future investigations on valley-related physics.

2. Fundamentals and theories of valley properties

2.1. Optical selection rules and valley Hall effect

Valley index is defined as a quantum number in crystals whose energy bands contain energetically degenerate but non-equivalent local maxima minima for valence bands or minima for conduction bands [6]. Generally, it is difficult to manipulate or control the carriers in one valley independently from another owing to the weak interactions with other external fields, which is completely different from spin. However, as illustrated in figure 2(a), in some materials such as ML-MX_2 with hexagonal lattice, the spatial inversion symmetry is broken. Thus, in the first Brillouin zone of ML-MX_2, there are inequivalent K^+ and K^- valleys with degenerate energy. The heavy elements and outer d-orbitals of MX_2 result in the strong spin–orbit coupling (SOC) and large spin splitting (figure 2(b)), with their valley polarization controllable by spin injection or vice versa.

Because of the inversion symmetry broken of crystal structures in ML TMDs, the Berry curvature and orbital magnetic moment at K^+ and K^- valleys are non-equivalent. As a result,
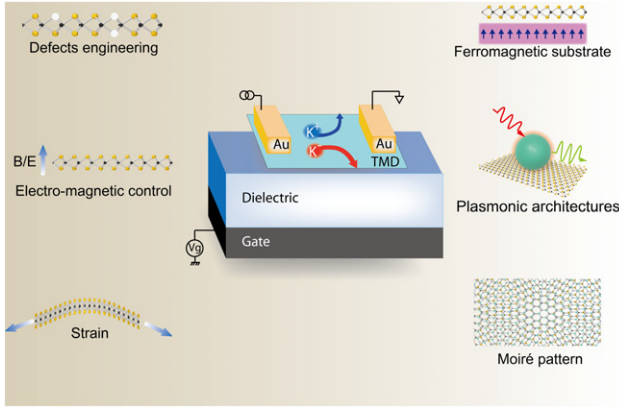
Figure 1. Schematic illustration of the different strategies for manipulating valley degree of freedom in ML-TMDs and hybrid heterostructures.

the valley states can be distinguished by electric or magnetic field, respectively [6, 15, 34]. The $\mathbf{k} \cdot \mathbf{p}$ Hamiltonian at the band edges in the vicinity of K^+ and K^- points is given by

$$\widehat{H} = dm \left(nk_x \sigma_x + k_y \sigma_y \right) + \frac{\Delta}{2} \sigma_z, \qquad (1)$$

where d is the lattice interval, m is the nearest neighbor hopping integral, $n = \pm 1$ is the valley index, σ is the Pauli matrix element and Δ is the bandgap [6, 10, 35]. In this regard, the Berry curvature for the conduction band is:

$$\Omega_c(k) = -\widehat{z} \frac{2d^2 m^2 \Delta}{(4d^2 m^2 k^2 + \Delta^2)^{3/2}} n, \qquad (2)$$

and the values of orbital magnetic moment for the valance and conduction bands is:

$$\mathbf{m}(k) = -\widehat{z} \frac{2d^2 m^2 \Delta}{4d^2 m^2 k^2 + \Delta^2} \frac{e}{2\hbar} n \qquad (3)$$

[6, 10, 35]. The different valley index ($n = \pm 1$) gives rise to non-zero and contrasting $\Omega_c(k)$ and $\mathbf{m}$, resulting in a series of valley effects. One of the effects of finite orbital magnetic moment is valley optical selection rules at K^+ and K^- valleys as depicted in figure 2(c) [34]. When subjected to a circularly polarized light, the carriers from each valley branch would be excited while keeping their valley-selective opposite orbital magnetic moments, leading to valley-selective circular dichroism. The inter-band transition at K^+ and K^- valleys couples only to right or left circularly polarized lights, respectively, which endures the optical modulation, propagation, and detection of valley polarization [9, 13, 36]. This valley optical selection rules resemble the spin optical selection rules in III–V semiconductors [37].

On the other hand, valley contrasting Berry curvature suggests that the carriers from diverse valleys could be driven by an in-plane electric field and propagate along contrasted transverse directions, resulting in a valley dependent Hall current, which is known as the valley Hall effect (figure 2(d)) [38, 39]. Because of the spin–valley locking, valley Hall effect can also be linked to spin Hall effect in ML-TMDs and van der Waals heterostructures [40–42]. Therefore, the coupling

between the valley pseudospin and external magnetic fields reveals potential use for information processing and storage [43, 44].

Besides ML TMDs, the inversion-symmetric bilayer TMDs could also exhibit large degree of spin/valley polarization. This phenomenon is probably attributed to the fact that excitons are localized in each layer of bilayer rather than spread over two layers. Since the inversion-symmetry is preserved in 2H-stacked bilayer TMDs, valley polarization should be smaller than ML TMDs. Therefore, people use electric field or other approaches to break the inversion symmetry in bilayer TMDs with a sizable valley contrasting Berry curvature, orbital magnetic moment, and optical circular dichroism [18, 19, 45, 46]. However, a few reports have shown that the degree of valley polarization in bilayer or multilayer WS_2 is much larger than that of ML WS_2 [47, 48]. Zhu *et al* observed the degree of valley polarization in bilayer WS_2 can be almost 100% at 10 K and decrease to ∼60% at room temperature. This anomalous behavior might be understood as the consequence of (i) coupling of spin, layer and valley degree of freedom, (ii) decoupled layer with suppressed interlayer hopping energy, and (iii) suppressed phonon assisted intervalley scattering through K^+–Γ–$K^+(K^-)$ channels due to increase of energy difference between the $K^+(K^-)$ and Γ valley for multilayers. Note that this anomalous phenomenon was not observed in bilayer or multilayer WSe_2 even though they have similar band structures to WS_2 [49].

2.2. Valley polarization

As mentioned above, the direct bandgap and the valley-contrast optical selection rules in ML-TMDs provide a simple method to modulate valley degree of freedom. The degree of valley polarization can be depicted by

$$\rho = \frac{I(\sigma^+) - I(\sigma^-)}{I(\sigma^+) + I(\sigma^-)}, \qquad (4)$$

where $I(\sigma^-)$ and $I(\sigma^+)$ are the left and right-handed circularly polarized PL intensities, respectively [8]. In a simplified picture, the steady-state valley polarization ρ can be expressed as

$$\rho = \rho_0 (1 - \delta)^2 / (1 + 2\tau_e/\tau_v), \qquad (5)$$

where ρ_0 is the theoretical degree of valley polarization, $1 - \delta$ refers to selectivity in the initial excitation (including possible intervalley generation) with $0 < \delta < 1$, τ_e is the exciton lifetime, and τ_v is the intervalley scattering time (valley lifetime). $\rho_0 (1 - \delta)^2$ is the initial valley polarization. We have $\delta = \delta_{imp} + \delta_{ph}$ to account for impurity/defects/substrate- and phonon-assisted excitation and recombination effects that lead to intervalley mixing from finite-momentum scattering [15]. The theoretical degree of valley polarization ρ_0 is constant for a given material at a fixed temperature. By time-resolved circularly polarized luminescence measurements, one obtains the initial valley polarization $\rho_0 (1 - \delta)^2$ when $\tau_e = 0$ s. One could thus get the value of selectivity in the initial excitation $1 - \delta$. Exciton lifetime τ_e is composed by the radiative lifetime τ_r
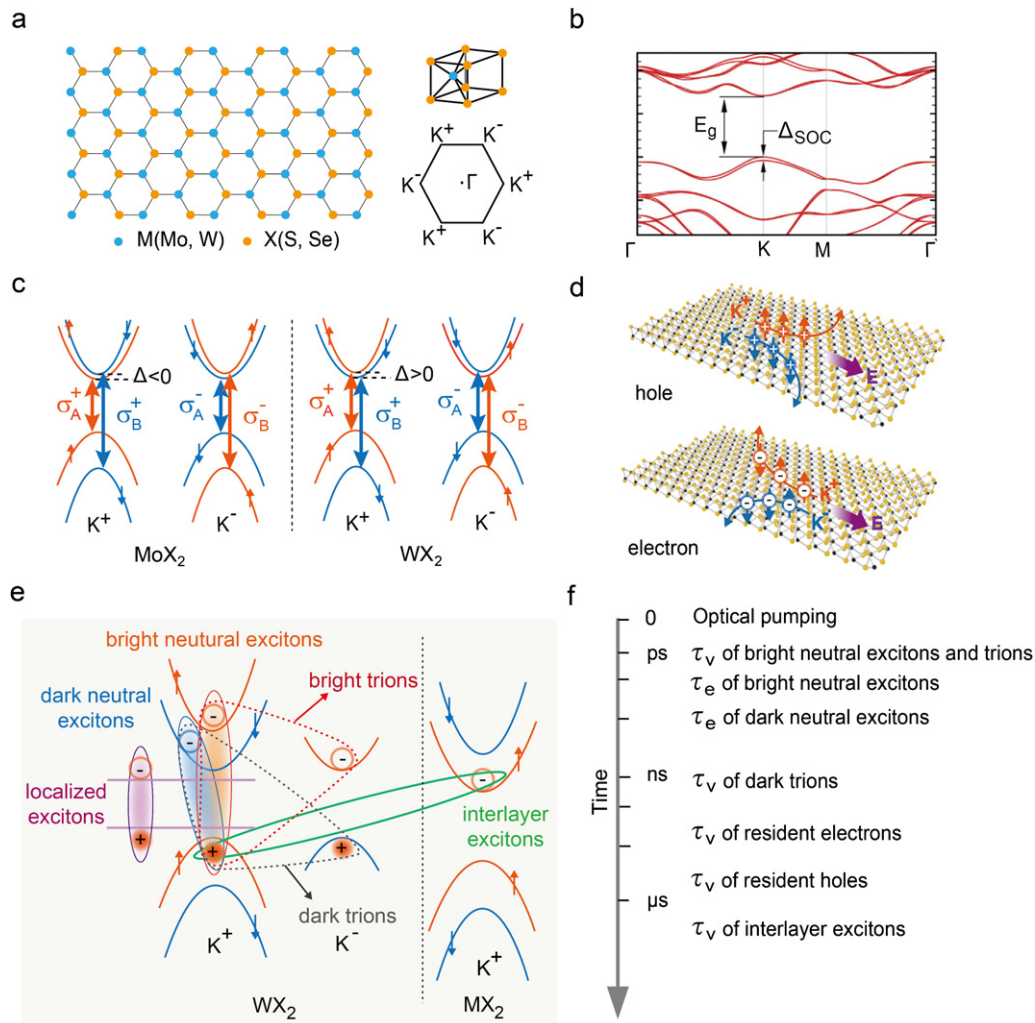
Figure 2. (a) Crystal structure of ML-MX$_2$ with hexagonal lattice. (b) The calculated band structure for ML-MX$_2$ by density functional theory, which shows the direct band gap along with the valence band splitting. Reprinted figure with permission from [50]. Copyright (2012) by the American Physical Society. (c) Valley-dependent optical selection rules for MoX$_2$ and WX$_2$ compounds. (d) Schematic of the valley Hall effect for electrons and holes. (e) The schematic sketch of different types of excitons in ML-TMDs and van der Waals heterobilayers. (f) Lifetime and valley lifetime scales for different types of excitations in ML-TMDs and heterobilayers.

and non-radiative lifetime τ_{nr}:

$$\frac{1}{\tau_e} = \frac{1}{\tau_r} + \frac{1}{\tau_{nr}} \qquad (6)$$

[51]. From equation (5), the degree of valley polarization strongly correlates with the values of δ and τ_e/τ_v. In general, the change of valley polarization by different manipulating strategies originates from the modified values of δ, τ_e and τ_v, which reveal the corresponding mechanisms.

2.3. Excitons and their valley lifetimes

In addition to high degree of valley polarization, long valley lifetimes are also required in practical valleytronic devices. As previously discussed, valley polarization is determined by intervalley scattering time τ_v and exciton lifetimes as well. Therefore, tremendous progress has been made for investigating the valley lifetimes and exciton lifetimes in TMDs. Exciton is the bound state of electron–hole (e–h) pair excitation, which is a sort of quasi-particles. As schematically shown in

figure 2(e), there are many kinds of excitons in TMDs and they are introduced as below. Bright neutral excitons (X$_0$) are bound states of electrons and holes with parallel spins formed by the Coulomb interactions, which are optically active. X$_0$ exhibits the valley-selective circular dichroism due to the optical selection rules and should decay slowly because intervalley scattering requires a large momentum transfer accompanied by the spin-flip process [52]. However, the long-range e–h Coulomb interactions mix two valley states and efficiently switch the spin and valley indices of carriers between K^+ and K^- valleys in picoseconds, resulting in fast valley depolarization for bright neutral excitons or charged excitons (trions) [53–57].

In contrast to X$_0$, electrons and holes with antiparallel spins will form optically inaccessible dark neutral excitons (D$_0$). Intriguingly, the Coulomb-exchange effect has a tiny impact on D$_0$ because the intervalley scattering of D$_0$ requires the spin-flip process. Therefore, the valley lifetimes of the spin-forbidden D$_0$ are theoretically predicted and have been experimentally demonstrated to be several orders larger than X$_0$

Table 1. Valley lifetimes of different types of excitations in ML TMDs and heterobilayers.

Materials	Temperature	Types of excitations	Valley lifetimes	Exciton lifetimes	Reference
MoS_2	300 K	Bright neutral excitons	1.7 ps	3.2 ps	[25]
WS_2	10 K	Bright neutral excitons	2.5 ps	2.5 ps	[73]
WSe_2	4 K	Bright neutral excitons	6 ps	3 ps	[57]
WSe_2	4 K	Dark trions	60 ps	230 ps	[58]
WSe_2	—	Dark trions	4 ns	—	[59]
WS_2	8 K	Dark trions	5.4 ns	—	[60]
MoS_2	5 K	Electrons	3 ns	—	[74]
WSe_2	5 K	Electrons	130 ns	—	[65]
MoS_2	74 K	Holes	10 ps	—	[75]
WSe_2	30 K	Holes	1 ns	—	[63]
WSe_2	5 K	Holes	2 μs	—	[65]
WSe_2/MoS_2	10 K	Holes	40 μs	—	[64]
$WSe_2/MoSe_2$	20 K	Interlayer excitons	—	1.8 ns	[62]
$WSe_2/MoSe_2$	30 K	Interlayer excitons	40 ns	>10 ns	[61]
$WSe_2/MoSe_2$	2.3 K	Interlayer excitons	1 μs	>1 μs	[31]
WS_2-WSe_2	—	Interlayer excitons	20 μs	~100 ns	[30]
WSe_2	5 K	Localized excitons	1 μs	200 ns	[68]

[58–60]. Another approach to obtain long lifetimes is utilizing the IX in type II van der Waals heterobilayer TMDs, where the corresponding electrons and holes are separated within various layers and the Coulomb exchange interactions are strongly suppressed [30, 31, 61, 62]. In the same way, the reason of long valley lifetimes of resident electrons and holes (major carriers in doped ML TMDs and heterostructures) transferred from photocarriers is that the valley pseudospins of electrons and holes are not affected by long-range e–h Coulomb exchange interactions [63–65]. It is noteworthy that a recent research found the valley lifetimes of resident holes in WSe_2–MoS_2 could be more than 40 μs at low temperatures, which are much longer than those of IX [64].

Apart from the e–h Coulomb interaction mechanism, defects/impurities and phonon-assisted scattering are relevant to valley lifetimes as well [46, 66, 67]. Because of the existence of impurities/disorders/defects or strain in ML-TMDs, the free excitons can be trapped in local potential wells and form localized excitons. Even though the impacts of defects/impurities on degree of valley polarization are still controversial, valley lifetimes of defect-bound excitons could reach to microseconds, exceeding those of bright neutral and charged excitons [68]. Meanwhile, the defect related localized exciton emissions could also be used as single-phonon emitters and play key roles in quantum information processing [69–71].

Lifetime and valley lifetime scales for different types of excitations in ML-TMDs and heterobilayers are summarized in figure 2(f). Note that valley lifetimes of excitons and resident electrons or holes can be effectively tuned via electrostatic doping. It has been demonstrated that the valley lifetimes of IX in TMD heterobilayers can increase as the gate voltage and reach as long as 39 ± 2 ns at 60 V [61]. Table 1 shows the experimental measured values of the valley lifetimes for different excitations in TMDs. From which, we can see that IX and resident valley polarized holes have much longer valley lifetimes than others, which are promising in valley-related information storage and processing applications. In addition,

the exciton lifetimes for various kinds of excitons differ a lot as well. Generally speaking, dark excitons have much longer radiative lifetimes than bright excitons. In a bright exciton, the electron and the hole have antiparallel spins and can recombine easily through the emission of a photon. In a dark exciton, the spins are parallel and the recombination cannot occur via direct emission of a photon as this would not allow for spin momentum conservation. IX are composed by electrons and holes separated spatially in heterobilayers. Because of the reduced overlap of the electron and hole wavefunctions in the IX, the lifetimes of IX can be much longer than intralayer excitons. Benefited from the long-lived IX, strong correlated states of excitons such as Bose–Einstein condensation and superfluidity could be formed even at room temperature [72].

3. Manipulation of valley polarization in monolayer TMDS

Based on equations (4) and (5), the optically generated exciton valley polarization is related to intervalley scattering between K^+ and K^- valleys and could be determined through measuring the PL intensities excited by left and right-handed circularly polarized light. Many attempts have been made to improve the valley helicity of ML-TMD by different methods. In this part, we would summarize the different engineering strategies on valley polarization of ML-TMDs and review the recent progress.

3.1. Optical pumping

As shown in figure 3, the experimental exploration of valley manipulation in TMDs can be traced back to 2012, when a few groups utilized circularly polarized resonant excitation to populate valley-polarized A and B excitons. The optical selection rules correspond to distinctly different PL spectra of ML MoS_2 with left and right-handed circularly polarized excitation [76]. Zeng *et al* have observed that the degree of valley polarization is sensitive to temperature. The PL polarization increases as
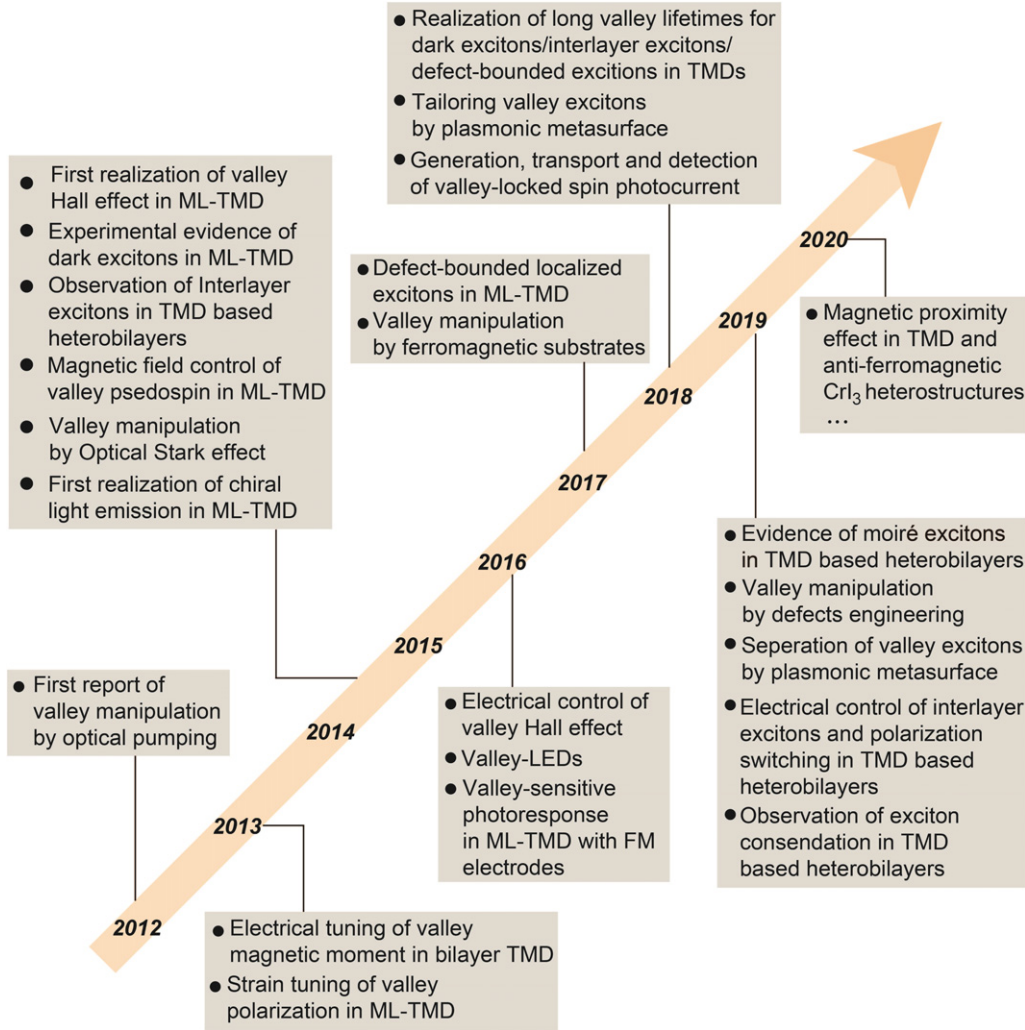
Figure 3. Timeline showing critical events in the development of valley manipulation in ML TMDs and hybrid heterostructures.

the temperature decreases until about 90 K and maintains constant at below 90 K due to the enhanced intervalley scattering and deviation of energy of resonance excitation when the temperature increases [16]. Thus, in order to obtain high degree of valley polarization, measurements at low temperature is essential. In addition, similar works have also proven, using optical pumping, that the degree of valley polarization in ML TMDs can be tuned to about 100% and 50%, by Mak *et al* and Cao *et al*, respectively [8, 15].

The optical selection rules can also be effective even for non-resonant excitations, which are known as optical Stark effects. Towards employing the optical selection rules in ML-TMDs, the optical Stark effect can be selectively exploited to valley-polarized excitons and separate valley states without applying magnetic field. By pumping with an ultrafast circularly polarized laser pulse, Sie *et al* have observed that an energy shift of 18 meV for the valley-polarized exciton in ML-WS$_2$ through the optical Stark effect [77]. This value of valley splitting would require a magnetic field of about 90 T for TMDs. Similarly, the valley-selective optical Stark effects can also be observed in ML WSe$_2$ and MoS$_2$ [78, 79]. The measured Stark shift is about 4 μeV for MoS$_2$, which is much

smaller than those of other TMDs. Recently, coherent control of the valley degree of freedom in ML-TMDs by applying the valley-specific optical Stark effect has been demonstrated and is promising for information processing in valleytronics [13].

3.2. Magnetic field

The energies of particles in the K^+ and K^- valleys are degenerate because the time-reversal symmetry is maintained in ML TMDs. However, this degeneracy can be broken with energy shift for electronic states under an magnetic field, which is known as valley Zeeman effect [80]. Valley pseudospin, analogous to real spin, can also be manipulated by magnetic field via orbital magnetic moment [21, 22, 80–84]. Because of the equal but opposite sign of the orbital magnetic moment of the two valleys and unequal orbital magnetic moment of conduction and valence band states in the same valley, the broken degeneracy of the valley excitons occurs [85–88]. The corresponding exciton valley *g* factor can be defined as

$$g = \frac{2(E_+ - E_-)}{\mu_B B}, \tag{7}$$

where E_+ and E_- are the measured exciton peak energy under left and right circularly light [81, 82]. The obtained exciton valley g factors are about -4, which are nearly consistent with the values that from the d-orbital contribution to exciton magnetic moment. The helicity of the splitting exciton peaks can switch as the sign of the direction of magnetic field, which results in contrast slope of polarization [21]. The linear Zeeman splitting for neutral excitons of ML TMDs are discernible $(0.1$–0.2 meV T$^{-1})$ [80]. Interestingly, the Zeeman splitting for trions is the same as neutral excitons in ML MoSe$_2$ while larger than neutral excitons in WSe$_2$ [80, 82]. Since the trion Zeeman splitting is strongly dependent on the gate voltage or carrier density, the different behavior of trion Zeeman splitting may originate from the different carrier density of various samples [82]. With the help of the splitting and broken of valley degeneracy in the applied magnetic field, the initial valley polarization ρ_0 in ML-TMDs is able to be further controlled.

3.3. Electrostatic doping

In order to help understanding the mechanisms of modulating valley polarization, we have described the energy band structures and possible scattering and exciton recombination pathways in figure 4(e). Equation (5) tells us the degree of valley polarization is proportional to intervalley scattering time τ_v and inversely proportional to exciton lifetime τ_e. The intervalley scattering include spin-conserving and spin-flip intervalley scattering. Since the spin-flip intervalley scattering needs both spin and valley flip, the scattering rate is likely small. In the present of large spin–orbit splitting of valence band in ML TMDs, K^+–K^- intervalley scattering of holes must flip spin (opposite to cases of electrons in conduction band), restricting the accessible relaxation pathways and thus enlarging τ_v. Therefore, it has been proposed that the spin-valley dynamics in ML-TMDs should strongly correlate with the electrostatic doping [11, 34]. Theoretical and experimental studies have demonstrated the long-range e–h exchange interactions govern the intervalley scattering process of exciton by the Maialle–Silva–Sham mechanism and result in a short valley lifetime (ps) [53, 57, 89]. Screening effect induced by electrostatic doping can efficiently suppress the long-range e-h exchange interactions in ML-TMDs and give rise to larger τ_v and ρ, while has no effect on τ_e [90–93]. Figures 4(a) and (b) clearly show the measured ρ and τ_v of ML-WSe$_2$ increase as the carrier density becomes larger [23]. Besides, similar experimental results also show that ρ of ML-WS$_2$ and ML-MoS$_2$ can be tuned by gate voltages at different temperatures, demonstrating a great influence of screening effect induced by electrostatic doping [94, 95].

In addition to long-range e–h exchange interactions, electron–phonon interaction is another key factor for valley depolarization. In polar crystals (such as TMDs), Fröhlich interactions couple longitudinal optical phonons to excitons or electrons and can be strongly restrained by electron heavy doping [96]. Therefore, this screening effect can also contribute to an enhanced degree of valley polarization in ML-MoS$_2$ [94].

3.4. Defects engineering

Because δ in equation (5) represent defects/impurity/substrate-related and phonon-assisted recombination effects that result in intervalley mixing from finite-momentum scattering, the degree of valley polarization ρ is expected to increase with decreasing defect density and temperature [53]. However, defects also have strong correlations with exciton lifetimes and intervalley scattering times, which have opposite impacts on ρ. Therefore, the role of defects in manipulating valley polarization is complicated. As schematically shown in figure 4(c), electron-beam irradiation is a kind of techniques that can create chalcogen vacancies in pristine ML-TMDs. The free excitons in ML-WSe$_2$ bound to low-energy defects and give rise to long recombination lifetimes ($\sim$200 ns), ultralong intervalley scattering time ($\sim$1 μs) and large degree of valley polarization (figure 4(d)). Therefore, in the absence of intervalley scattering, this disordered WSe$_2$ shows robust valley polarization and large valley-selective circular dichroism [68].

Chemical vapor deposition (CVD) is another technique to induce spontaneous defects in as-grown ML-TMDs, providing platforms for investigating the relationship between defects and valley polarization [26, 97–100]. For example, even though the exciton lifetimes of S-vacancies are longer than those of W-vacancies, the less defect density in domains with S-vacancies result in less intervalley scattering and larger valley polarization than domains with W-vacancies [26]. The phenomena that hybridization between excitons and defects reducing the degree of valley polarization has also been theoretically predicted and experimentally demonstrated [101, 102].

However, some recent experimental results are quite opposite to that mentioned above. The defects in MoS$_2$ could be passivated by laser irradiation under ambient via H$_2$O molecules, diminishing the nonradiative recombination centers and degree of valley polarization [68]. Additionally, the ML-WS$_2$ and WSe$_2$ grown by McCreary et al also exhibit different correlations between defects/disorders and valley polarization. They experimentally proved that higher degree of sample disorders arising from defects attributes to shorter nonradiative lifetimes, which is responsible for higher degree of valley polarization (figure 4(f)) [27].

Eventually, the disparity of valley polarization among the results originates from the competition between the parameter δ and τ_e/τ_v in equation (5). Even though the role of defects in TMDs seems still ambiguous, the ability to modulate the valley polarization through defects engineering paves a new way for tailoring valleytronic properties of TMDs.

3.5. Strain engineering

Mechanical strain is another approach that can tune the valley polarization of TMDs. For example, it has been demonstrated that valley polarization of ML MoS$_2$ decreases as the tensile uniaxial strain increases [103]. This is because more holes in MoS$_2$ scatter from the K to the spin degenerate Γ valley after absorption of photons and indirect transition from the valence to the conduction band [104]. Besides the applied uniaxial strain by bending TMDs, a moderate tensile strain can also be
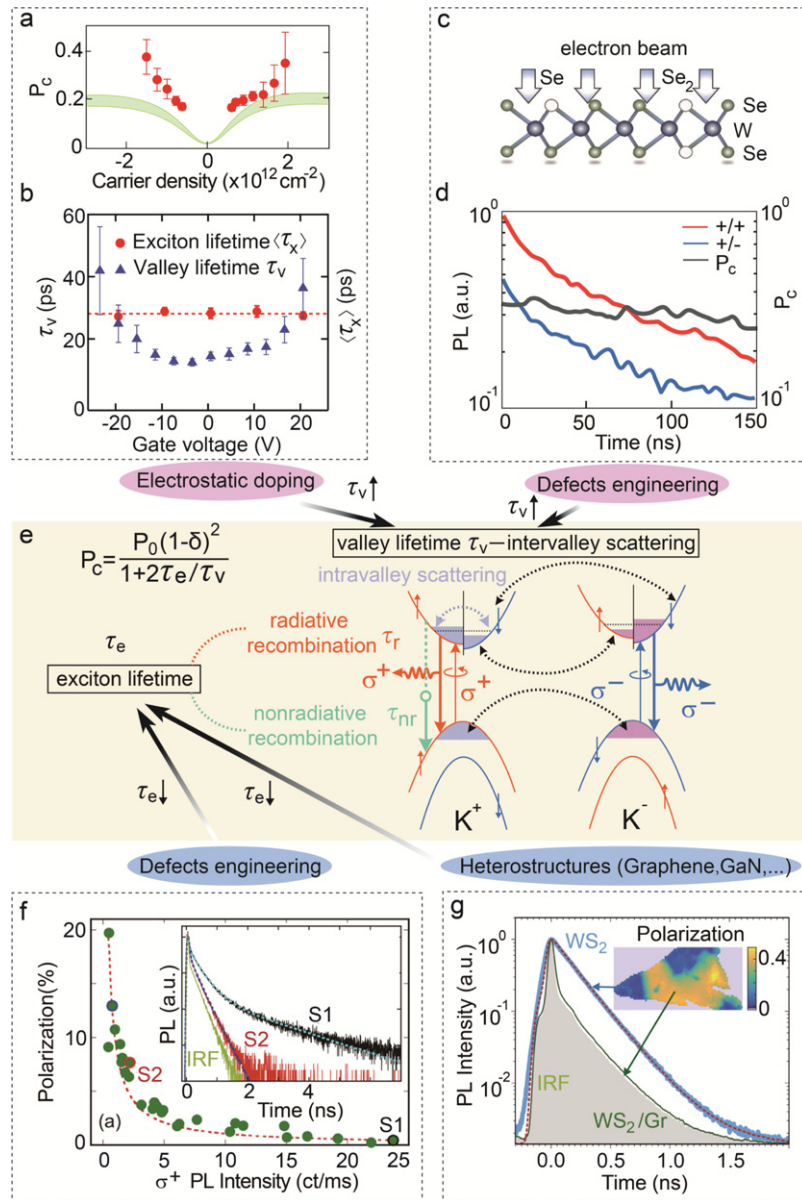
Figure 4. Some typical mechanisms of tailoring the degree of valley polarization in TMDs. (a) The dependence of valley polarization for excitons in ML-WSe$_2$ on the carrier density. The red dots are measured results and the green regions represent the calculated values. (b) The extracted valley lifetimes (blue triangles) and exciton lifetimes (red circles) as a function of gate voltages. [23] John Wiley & Sons. © 2019 WILEY-VCH Verlag GmbH & Co. KGaA, Weinheim. (c) Two kinds of selenium vacancy (Se$_1$ and Se$_2$) in ML-WSe$_2$ created by electron-beam irradiation. (d) Time-resolved circularly polarized emission and the degree of valley polarization P_c (gray lines). Reprinted figure with permission from [68]. Copyright (2018) by the American Physical Society. (e) The diagrams of band structures and available scattering and recombination pathways in WX$_2$. The intervalley scattering time of valley polarized particles and quasi-particles is defined as valley lifetimes. Exciton lifetimes consist of radiative and non-radiative recombination times. By tuning valley and exciton lifetimes through electrostatic doping, defects engineering and constructing heterostructures, the degree of valley polarization in TMDs is able to be enhanced. (f) The dependence of degree of valley polarizations and PL emission intensities obtained by measuring several CVD-grown WS$_2$ samples (including S1 and S2). The inset is time-resolved PL emissions of S1 and S2. Reprinted with permission from [27], Copyright (2017) American Chemical Society. (g) Time-resolved PL emissions of WS$_2$ and WS$_2$/graphene heterostructures. The inset is the mapping of the degree of valley polarization for WS$_2$ and WS$_2$/graphene heterostructures. Reprinted with permission from [24], Copyright (2018) American Chemical Society.

induced by the mismatch of lattice constant between ML TMDs and other epitaxial substrates. Theoretical analysis predicted that the valley polarization has a strong correlation with the strain in the WS$_2$/MnO and MoTe$_2$/EuO heterostructure [105, 106]. Since ML-TMDs possess mechanical flexibility, there is no doubt that strain modulated valley polarization is attractive and practical for promising flexible applications.

4. Valley manipulation in hybrid heterostructures based on TMDs

The quasiparticle interactions between TMDs and other functional materials (0D–3D) could introduce novel interfacial effects, such as carrier transferring, proximity effects and electron–phonon coupling, etc. These interfacial effects may

provide addition routes to tune the valley polarization in TMDs in spite of the external fields or conditions. For instance, in the ML-TMD/graphene hybrid systems, because of the highly efficient interlayer coupling, the photo-induced e–h pairs are dissociated by the build-in internal electric field between graphene and ML-TMD and give rise to ultrashort lifetimes of excitons ($\leqslant 1$ ps), which result in a high degree of valley polarization up to 0.4 at room temperature (figure 4(g)) [24]. Additionally, the lifetimes of valley polarized excitons can also be decreased through the energy dissipation induced by electron–phonon interactions in the MoS_2/GaN heterostructure. The valley helicity at room temperature is accordingly enhanced to about 0.33 [25]. Therefore, the importance of hybrid heterostructure engineering for manipulating valley polarization in TMDs is highlighted. In this part, we would review the current work to discuss the different mechanisms of valley manipulation by engineering the interfacial effects between TMDs and other materials.

4.1. ML-TMDs on ferromagnetic substrates

Because the valley splitting caused by external magnetic fields is often weak (0.1–0.2 meV T^{-1}), large degree of valley polarization needs very high magnetic field. In order to overcome this, researchers have been seeking methods for increasing the valley splitting in ML-TMDs. Exploiting the proximity effect from FM substrates to induce interfacial magnetic exchange field in ML-TMDs may be a solution (figures 5(a) and (b)). An enormous valley splitting of 2.5 meV at 1 T for ML-WSe_2 on EuS substrate and up to 19 meV above 3 T for ML-WS_2 on EuS substrate at 7 K have been demonstrated by Zeng et al (figure 5(c)) [28, 29]. Apart from EuS substrates, a large magnetic exchange field could also be generated at the interface of ML-TMDs and yttrium iron garnet, giving rise to a large degree of valley polarization ($\sim$70%) for trions in ML-MoS_2 [107].

Recently, 2D magnetic materials have inspired tremendous attentions and brought opportunities for next-generation spintronic devices due to no lattice distortion, least interfacial damage and flexibility of stack order and twist angle [109–116]. Among the van der Waals magnetic materials, odd-layer CrI_3 is a kind of FM insulator with out-of-plane magnetization direction under about 60 K and its magnetism can be tuned by electrostatic doping [111, 117]. Zhong et al have indeed experimentally detected a large valley splitting of as large as 150 meV T^{-1} in ML-WSe_2 and CrI_3 van der Waals heterostructrues and found that the valley polarization can be rapidly switched by changing the magnetization orientation of CrI_3 (figure 5(d)) [108]. Note that the sign of valley polarization ρ also changes near ± 0.85 T, which is extremely intriguing because the external magnetic field has not flipped. This unusual result is possibly originated from the photo-induced flipping of spins in CrI_3, giving rise to the manipulation of the valley polarization and splitting of WSe_2 [118].

4.2. Plasmonic architectures

It is well known that surface plasmon resonance can concentrate light in a tiny volume, leading to the enhancement of electromagnetic fields and the boost of light–matter interactions [119–121]. Therefore, the quantum efficiency and PL intensity of TMDs can be improved via Purcell effect by introducing plasmonic nanostructures. However, controlling valley polarization in TMDs needs extreme careful tailoring of the electromagnetic near fields, particularly in terms of chirality. To achieve such a chiral electromagnetic near field, chiral plasmonic nanostructures are suggested as promising candidates, as demonstrated in highly sensitive optical detection of chiral biomolecule [122–124]. Recently, a number of chiral plasmonic nanostructures have been used to modulate valley polarization in ML TMDs ((figure 5(e)) [125–132].

Li et al have demonstrated a system composed of a CVD-grown ML MoS_2 sandwiched between a chiral plasmonic nanostructure and a gold film, as shown in figure 5(f). The chiral plasmonic nanostructure is composed of periodic arrays of nanorods with a C4 symmetric unit cell. By introducing chiral plasmonic nanostructure, the degree of valley polarization in ML MoS_2 can be either improved from 25% to 43% with excitation of left circularly polarized light or reduced from 25% to 20% with excitation of right circularly polarized light. They show that the change of valley polarization is mainly due to the fact that the generation and recombination rates of excitons in K^+ and K^- valley are efficiently enhanced and suppressed, respectively (Figure 5(f)) [32].

However, the chiral performance was only successfully achieved at 87 K due to the low coupling efficiency between the valley excitons in MoS_2 and metasurfaces. Wu et al recently demonstrated that moiré chiral metamaterials (MCMs) can efficiently tailor valley-polarized PL of ML WSe_2 at room temperature [133]. As shown in figure 5(g), MCM is composed of two layers of periodic Au nanoholes with a controlled interlayer in-plane rotation angle θ and a dielectric spacer. A ML WSe_2 is embedded between the dielectric spacer and the top Au nanohole array of MCM. Due to the θ-induced mirror symmetry breaking, the near field within the spacer of metal–insulator–metal (MIM) structure exhibits strong dependence on chirality of the incident light. The near field in the MIM structure can modulate the spontaneous decay of excitons in dependence of spin via chiral Purcell effect, and thus, the degree of valley polarization in the WSe_2-MCM hybrid structure. By taking advantage of the chiral coupling between ML-TMDs and plasmonic architectures, a prototype of room-temperature valleytronic transistor has been experimentally demonstrated, providing a universal method to encode and process information by valley degree of freedom at room temperature [134].

4.3. Moiré patterns

Recently, the emergence of moiré excitons with unique valley-polarized properties has attracted enormous attention. Moiré exciton is a kind of IX that trapped in moiré potentials, which is induced from stacking two atomically thin 2D materials (figures 6(a) and (b)) [135]. The moiré potential has been demonstrated to induce abundant physics, such as superconducting in twisted graphene [136–139] and IX in TMD heterobilayers [61, 140–145]. Note that the IX show different
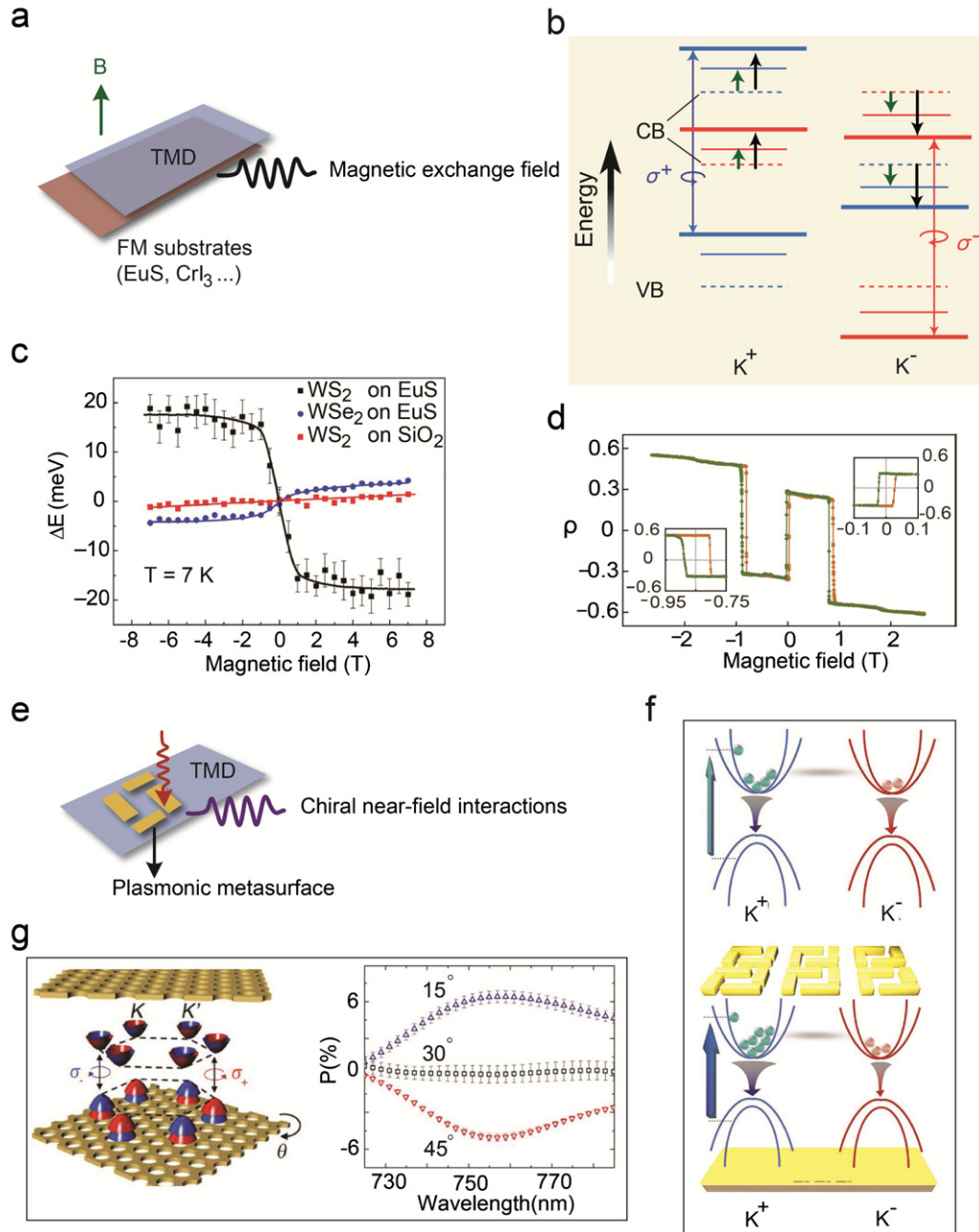
Figure 5. Modulating valley polarization of TMDs by interfacial effects between ML-TMDs and FM substrates/plasmonic metasurface. (a) Schematic of magnetic exchange field at the interface of ML-TMDs and FM substrates (such as EuS and 2D layered CrI_3). (b) The sketch of band shifts for ML-TMDs (thin solid lines) and ML-TMDs on FM substrates (thick solid lines) under the same magnetic field. The dashed lines represent the band diagram before applying the magnetic field. (c) Different valley Zeeman splitting of WS_2 on SiO_2, WS_2 on EuS, and WSe_2 on EuS at 7 K. Adapted by permission from Springer Nature Customer Service Centre GmbH: Nature Communications [29], © 2019. (d) Degree of valley polarization when magnetic field sweeps up (orange) and down (green). From [108]. Reprinted with permission from AAAS. (e) Schematic of chiral near-field interactions at the interface of ML-TMDs and plasmonic metasurface. (f) Band diagrams of ML-MoS_2 (top) and MoS_2-metasurface (bottom). [32] John Wiley & Sons. © 2018 WILEY-VCH Verlag GmbH & Co. KGaA, Weinheim. (g) Left: the sketch of the WSe_2-MCM hybrid heterostructures. Right: degree of valley polarization in WSe_2-MCM hybrid structures with different in-plane rotation angles. [133] John Wiley & Sons. © 2019 WILEY-VCH Verlag GmbH & Co. KGaA, Weinheim.

properties compared with excitons in ML-TMDs. For example, a large effective g factor of -15 and a high degree of the valley polarization of over 80 % at 30 T can be observed for the IX in the AB-stacked $MoSe_2$–WSe_2 heterobilayer [146]. Furthermore, the valley diffusion length could exceed 20 μm in the WS_2–WSe_2 heterobilayer, which is drastically promising for the exciton devices [30]. The valley lifetimes

of IX in the WS_2–WSe_2 heterobilayer can reach up to 20 μs, which are several orders longer than those in ML-TMDs (shown in table 1) [30].

The mechanism of moiré patterns engineering valley polarization is that the relative location between Mo and W atoms (A, B and C sites) could give rise to different optical selection rules of excitons within the supercell (figure 6(c)), which has
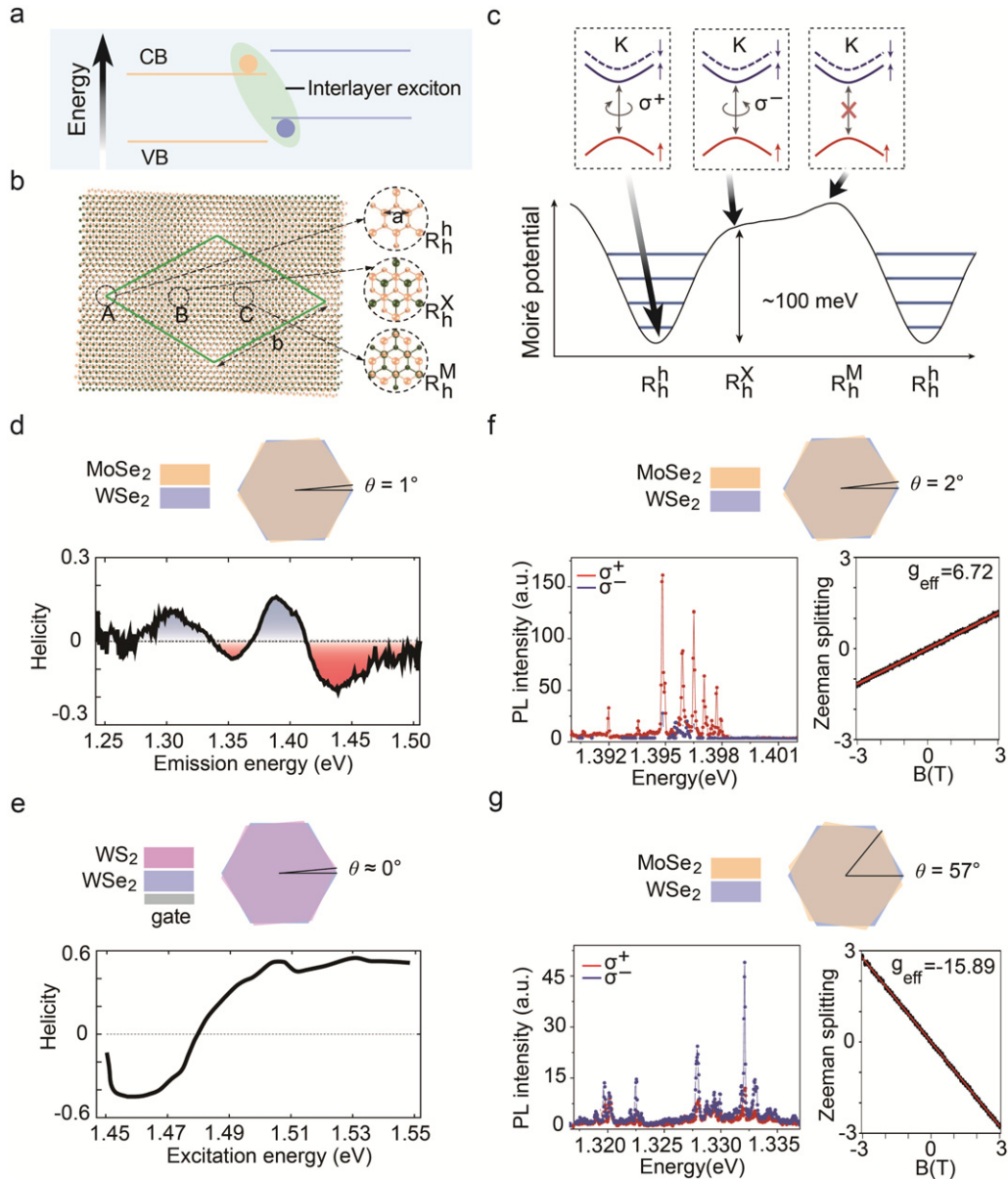
Figure 6. Modulating valley polarization of ML-TMDs by moiré potentials. (a) Type II band alignments and schematic of interlayer excitons by stacking TMD heterobilayers. (b) Moiré pattern in the MoX_2/WX_2 heterostructure with a long period. A, B and C are different R-type stacking. From [135]. Reprinted with permission from AAAS. (c) Different moiré potentials and optical selection rules for interlayer excitons at A, B and C sites. (d) The sketch of $MoSe_2/WSe_2$ heterobilayer with twist angle of $1°$ (top) and the corresponding PL helicity as a function of emission energy (bottom). Adapted by permission from Springer Nature Customer Service Centre GmbH: Nature [142] © 2019. (e) The sketch of WSe_2/WS_2 heterobilayer with twist angle of $0°$ (top) and the corresponding PL helicity as a function of excitation energy (bottom). Adapted by permission from Springer Nature Customer Service Centre GmbH: Nature. Nature Physics [147] © 2019. Helicity-resolved PL spectra and Zeeman splitting in $MoSe_2/WSe_2$ heterobilayers with twist angles of $2°$ (f) and $57°$ (g). Adapted by permission from Springer Nature Customer Service Centre GmbH: Nature [143] © 2019.

been predicted by Yu *et al* [135]. Recently, these multiple interlayer exciton states and opposite optical selection rules at different moiré sites have been experimentally demonstrated in $MoSe_2/WSe_2$ heterobilayer with twist angle of $1°$ (figure 6(d)) and WSe_2/WS_2 moiré superlattice (figure 6(e)) [142, 147]. Moreover, Seyler *et al* have surprisingly found that quantum emitters in $MoSe_2/WSe_2$ heterobilayer also present high valley polarization [143]. The degree of valley polarization for heterobilayer with $57°$ is over 70% ((figure 6(f)), while the selection rule is reversed for heterobilayer with $2°$ (figure 6(g)).

The observed high circular polarization with different helicity suggests the IX trapped in moiré potentials.

In order to further optimize the strategies for valley manipulation, we have summarized the merits and shortcomings of different modulating methods in 2D valleytronic systems (table 2). In general, due to the easy excitation and detection through optical pumping, many works on valley polarization and valley lifetimes have been investigated. However, the degree of valley polarization decreases significantly as the temperature increases because the intervalley scattering is
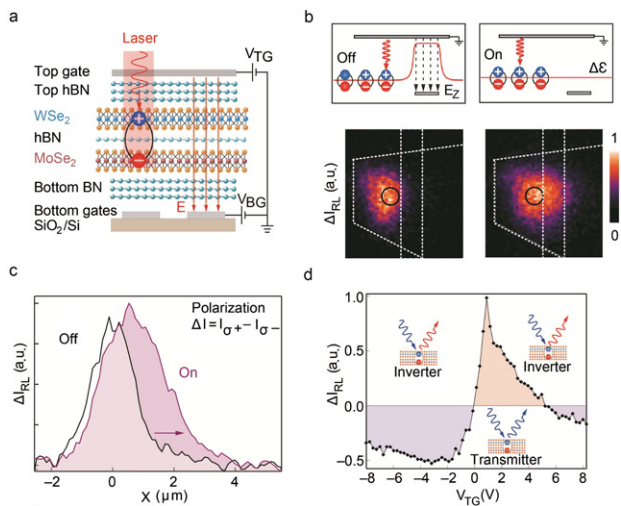
Table 2. Merits and shortcomings of various methods for modulating valley information in 2D materials.

Modulating methods	Merits	Shortcomings
Optical pumping	● Easy to initialize ● Easy to readout through photon polarization ● Near-unity valley polarization	● Short valley lifetime ● Low degree of valley polarization at room temperature
Magnetic field	● Easy to produce valley polarization ● Easy to tune the value of valley polarization	● Requirement for large magnetic field
Electrostatic doping	● Convenient for modulating valley properties ● Easy to change the type of exciton by doping ● Continuous modulation	● Difficult for precise control
Defects	● Easy to introduce by CVD or irradiation ● Large valley polarization even at room temperature	● Difficult to control the types and quantities ● Difficult to recover to previous states ● Bad repeatability
Strain	● Enable to be applied for flexible devices ● Inversion symmetry breaking ● Modifying both crystal and band structures	● Difficult to fabricate devices ● Difficult to measure the value of strain precisely
Ferromagnetic substrates	● Easy to produce valley polarization ● Easy to tune the value of valley polarization ● Large valley spitting and large degree of valley polarization	● Difficult to fabricate heterostuctures ● Some 2D layered ferromagnetic materials are easy to degrade under ambient conditions.
Moiré patterns	● Long exciton lifetime ● Long valley lifetime	● Difficult to fabricate heterostuctures with specific degrees ● Only observable for some specific twist angles
Plasmonic architectures	● Easy to modify valley exciton dynamics ● Enhancing light−matter interactions ● Enable to separate valley dependent excitons	● Complicated fabrication process

enhanced with the assistance of phonons at high temperatures. Therefore, the intrinsic values of valley polarization for ML-TMDs using optical pumping are usually low at high temperatures. Moreover, the valley lifetimes of bright excitons in ML-TMDs are short as well (table 1). Considering the relative low degree of valley polarization and short valley lifetimes at high temperatures, innovative strategies of tailoring valley polarization and valley lifetimes are expected to develop for the room-temperature valleytronic applications. External magnetic field can effectively produce and tune valley polarization. But the requirement of large magnetic field is difficult for integration of valleytronic device. Electrostatic doping by gate modulation is a convenient way for tuning the valley properties and is promising for electrically initializing and reading out valley information in valleytronic devices. Defects and strain engineering are difficult to precisely control and may degrade the valley polarization. In addition, hybrid heterostructures based on TMDs and FM substrates, moiré patterns, and plasmonic architectures offer new methods to obtain larger valley degree of freedom and longer valley lifetimes as shown in table 1 and figure 7 [8, 15, 16, 23, 24, 26, 27, 31, 32, 47, 61, 68, 76, 94, 95, 103, 107, 108, 133, 142, 146, 148–152]. Accordingly, a combination of multiple tuning methods on the valley properties may lead to unprecedented physical phenomena in TMDs.

5. Valleytronic devices

The interesting features of valley polarization in ML-TMDs and heterostructures enable numerous novel applications. In this section, we will introduce recent advancements in several

Figure 7. Summarization of the measured degree of valley polarization in TMDs and hybrid heterostructures as a function of temperature with different modulating strategies.

applications such as valley-switch, valley-photodetectors, and valley-light emitting diodes.

5.1. Valley-photonic devices

As we have introduced above, optical generation and control of valley polarization for TMD excitons have been intensely investigated. However, the exciton and valley polarization exhibit short lifetimes on the picosecond timescale in ML TMDs, imposing prohibitive restrictions on valley-photonic devices. Fortunately, IX formed in TMD heterostructures with ultralong radiative and valley depolarization lifetimes provide a way to overcome the limitations. As mentioned before, IX can be easily trapped in the local minima of the moiré potential and are difficult to diffuse or drift. In order to overcome this barrier, a 2D atomically thin spacer such as few-layered

Figure 8. Valley-photonic switch based on TMD heterobilayers. (a) Schematic illustration of the WSe_2/h-BN/$MoSe_2$ heterostructure with top and bottom gates. (b) Top: numerically simulated profile (red line) of the exciton energy, which exhibits the off ($V_{BG} = -7$ V) and on ($V_{BG} = 0$ V) states at $V_{TG} = 0$ V. Bottom: the corresponding spatial images of the exciton cloud polarization showing the off and on states. (c) Intensity profiles of polarization indicating the action of the valley-polarized excitonic transistor. Adapted by permission from Springer Nature Customer Service Centre GmbH: Nature Nanotechnology [153] © 2019. (d) Polarization switching operation at different top gate voltages in $MoSe_2$/WSe_2 heterobilayer. Adapted by permission from Springer Nature Customer Service Centre GmbH: Nature Photonics [150] © 2019.

h-BN can be introduced between two ML-TMDs and separate the electrons and holes (figure 8(a)). In this regard, the heterobilayer not only can allow the existence of long-range moiré pattern, but host IX as well. As schematic illustrated in figure 8(b), by controlling the energy of gate area higher or lower than its surroundings, exciton diffusion can be allowed or blocked [153]. At the same time, because IX can take valley information, the van der Waals heterostructrues can be used as a valley-polarized exaction transistor (figure 8(c)).

Similarly, Ciarrocchi *et al* have also realized a polarization switch of IX via modulating their moiré potentials [150]. The lower-energy interlayer exciton IX_1 and higher-energy interlayer exciton IX_2 in $MoSe_2$/WSe_2 heterobilayer have opposite helicity at positive gate (*n* doping). Therefore, through controlling the gate voltage, this device can behave as a polarization inverter as shown in figure 8(d). With this electrostatic tunable switching of the helicity state, a logic NOT gate can be realized, which is of great importance for logic operations.

5.2. Valley-photodetectors

Photodetectors based on 2D materials have attracted wide attention [154–160]. To fully meet the requirements of valleytronic devices, the optoelectronic generation of spin-valley locked carriers, spin transport and electrical readout are essential [161–167]. On one hand, for local measurements, lateral spin-valve-like structure with FM electrodes based on ML WS_2 can electrically detect the spin-polarized photocurrent induced by circularly polarized light (figure 9(a)) [168, 169]. The constructive scanning photocurrent patterns in figure 9(a)

obviously show the valley-selective circular dichroism when the direction of FM electrode magnetization is parallel or antiparallel with that of polarizations of photo induced carriers [168]. This phenomenon reflects that the photo-induced carriers in ML-TMDs comply with the valley-dependent optical selection rules and are spin-polarized due to spin-valley locking. On the other hand, for non-local measurements, graphene is a good candidate for spin transport layer owing to its weak spin–orbit coupling and long spin diffusion length [170–172]. Gmitra *et al* have previously predicted that ML MoS_2 can generate photo-induced spin-valley locked carriers and inject them into an adjacent graphene by absorbing circularly polarized light [173]. This prediction has been recently experimentally demonstrated in van der Waals heterostructures composed by ML-MoS_2 and graphene with FM electrodes [174]. The device structure and non-local measurement configuration are schematically shown in figure 9(b). When ML-MoS_2 is illuminated by the circularly light, the spin of photo-induced carriers is polarized. By applying a small magnetic field B_y, spin precession generates a finite component along the magnetized direction of FM electrode. The antisymmetric Hanle curves further confirm that the nonlocal voltage signal V_{NL} is indeed from the valley-locked spins from MoS_2.

Beyond FM electrodes, the topological insulators can also be utilized for the detection of the valley-spin locked electrons because of its particular properties, namely the spin-momentum locking [175–178]. Figure 9(c) presents the schematic of the valley(spin)-tronic device and the corresponding measured light-helicity-dependent non-local valley-spin locked photocurrent for WSe_2 by Bi_2Se_3 electrodes at different gate voltage [179]. But for local measurements, the capability of tuning valley polarization by gate is greatly weakened (figure 9(d)). The gate modulated spin injection, transport and detection is promising for valley(spin)-tronic devices. It is noteworthy that in addition to the FM electrodes and topological insulators, non-FM electrodes could also detect the valley-polarized photocurrent by inducing out-of-plane magnetic field or Zeeman effect, which has been recently demonstrated [180].

5.3. Valley-light emitting diodes

Opposite to tuning valley degree of freedom with optical helicity, inequivalent excitons of valleys can also be electrically populated and give rise to circular light emission. Because both WSe_2 and $MoSe_2$ show ambipolar conductive properties, lateral p–i–n homojunctions can be formed by ionic gating [181, 182]. As shown in figure 10(a), through changing the direction of current, the chirality of electroluminescence (EL) can be switched reversely, which is due to inequivalent overlap of the electron and hole states at each valley induced by trigonal warping effects. [181] In addition to the p–i–n homojunctions, p-Si/i-WS_2/n-ITO exhibit similar circular EL with valley polarization (figure 10(b)) [182, 183].

Spin can be effectively injected from FM electrodes into ML-TMDs (figure 10(c)) [184–187]. Optical transition rules are allowed for e–h pairs in the same valley and give rise to circular EL and an extra electron. In this regard, by controlling the direction of magnetization of FM electrode,
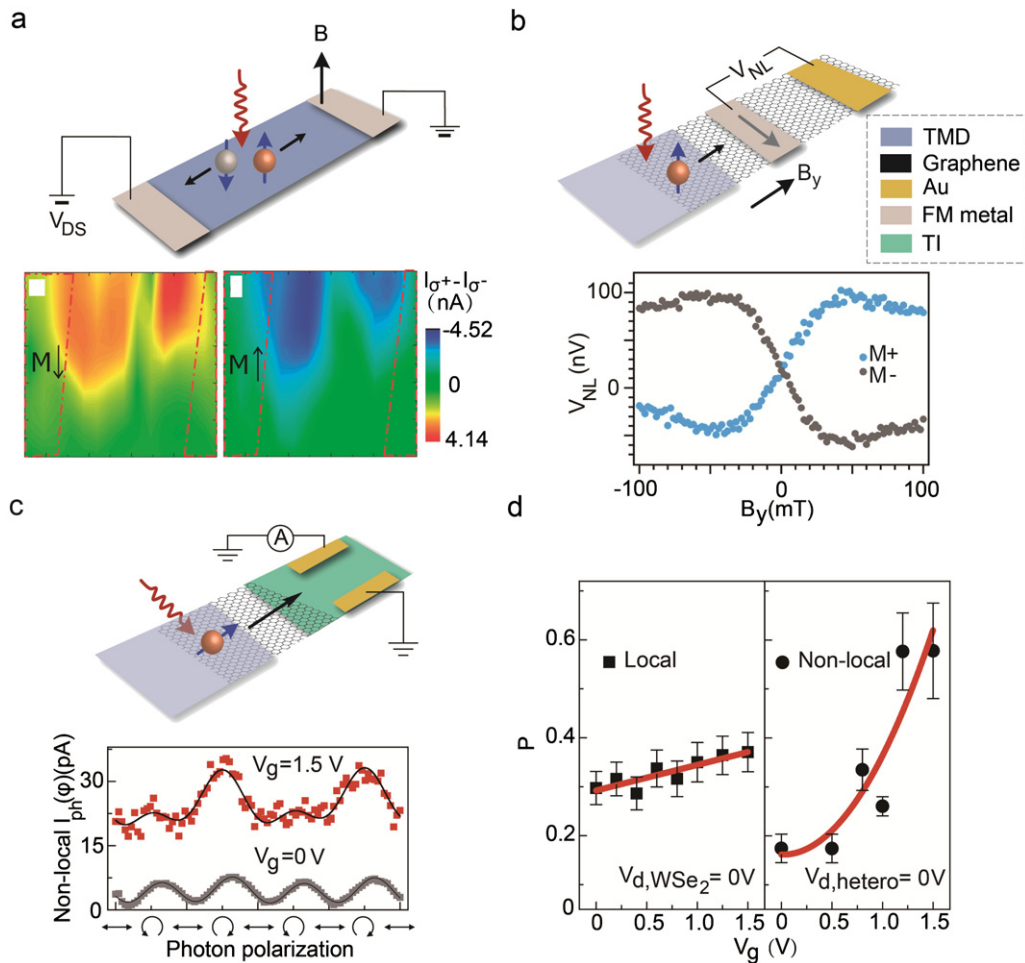
Figure 9. Valley-sensitive photodetectors based on ML-TMDs and heterostructures. (a) Schematic illustration of valley-polarized photocurrent measurements for ML-WS$_2$ (top) and the spatial mapping of photocurrents with contrast magnetized orientations of FM electrodes under zero external magnetic field. Reproduced with permission from [168]. © 2016 National Academy of Sciences. (b) Schematic of non-local spin-polarized photocurrent measurements in an ML-MoS$_2$/graphene heterostructure (top) and imparity of B_y-dependent spin signal V_{NL} by switching the magnetization orientation of FM electrodes (bottom). Reprinted with permission from [174]. Copyright (2017) American Chemical Society. (c) Top: schematic illustration of the non-local circular photogalvanic effect measurement. Bottom: the corresponding valley-dependent photocurrents at $V_{d,hetero} = 0$ V for $V_g = 0$ V (gray) and 1.5 V (red). (d) Gate-dependent degree of valley polarization through local and non-local measurements. Adapted by permission from Springer Nature Customer Service Centre GmbH: Nature Nanotechnology [179] © 2018.

interband transitions of ML TMDs involve the emission of valley polarized light and can be tuned by out-of-plane magnetic field as exhibited in figure 10(c) [188]. In addition to the FM electrodes, dilute magnetic semiconductors are another candidates for electrically injecting spins into ML TMD. Ye *et al* have observed circular EL in heterostructures based on ML-WS$_2$ and (Ga, Mn)As, as schematically represented in figure 10(d) [73]. The hysteresis helicity of EL is coincident with anomalous Hall effect of (Ga, Mn)As and indicates inequivalent population of two valleys, resulting in the formation of valley polarized excitons.

5.4. Other valleytronic devices

Other novel valleytronic devices such as valley-diodes and valley thermoelectric devices are very attractive both theoretically and experimentally. In analogy to spin diodes, implementation of valley-diodes requires that the current contributed by

a single valley through a junction should be simultaneously forward-conductive and reverse-blocking. Benefited from the specific band-matching mechanism, researchers have theoretically predicted that spin-valley diodes can be realized through group-IV ML FM-field/E_z-field junction [189, 190]. Moreover, uniaxial strain in ML MoS$_2$ can lead to unbalanced Berry curvatures centered at K and $-K$ points and thus valley magnetization under an external electric field, which has been experimentally discovered by Lee *et al* [191]. A real-space homogeneous distribution of the valley magnetization can be regarded as valley magnetic domains (K^+ and K^-). Recently, Kim *et al* found that anomalous transverse current could be generated by controlling the relative size of the valley magnetic domain. This anomalous transverse current flows toward only one direction along the movement of valley magnetic domain, which is possibly applied in valley-diodes [192].

Although adopting optical and electrical methods to realize valley-polarized effects has been widely studied, there are so
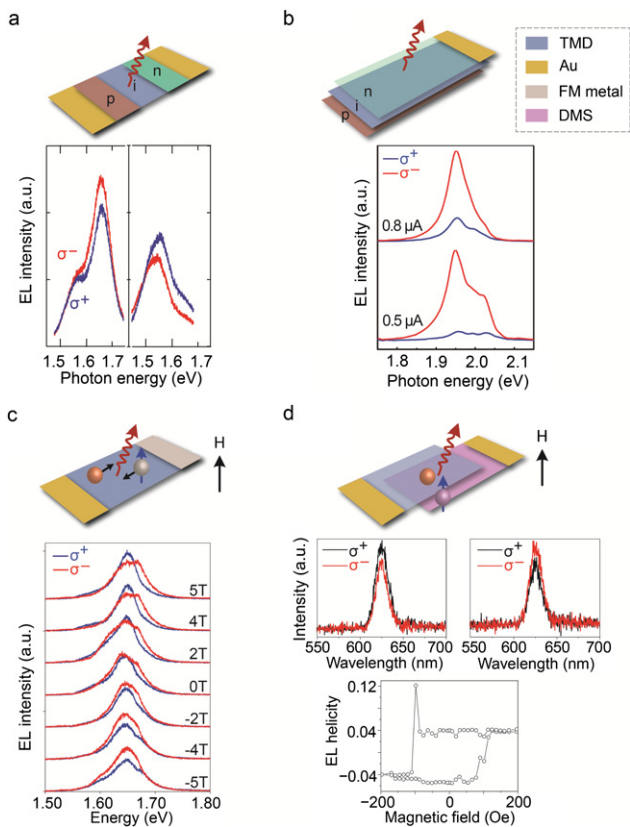
Figure 10. Different types of valley-light emitting diodes constructed by ML-TMDs and heterostructures. (a) Sketch of a lateral p–i–n homojunction of ML-TMD through ionic gating (top) and corresponding helicity-resolved EL spectra of ML-WSe$_2$. From [181]. Reprinted with permission from AAAS. (b) Schematics of a p–i–n heterojunction (top) and circularly polarized EL spectra under different applied currents (bottom). Reprinted with permission from [183]. Copyright (2016) American Chemical Society. (c) Sketch of a heterostructure composed of ML-TMD and FM electrodes that can inject spin-polarized holes and emit helicity-resolved light (top) and the corresponding EL spectra of the device at different magnetic fields (bottom). Reprinted with permission from [188]. Copyright (2016) American Chemical Society. (d) Schematic of a heterostructure composed of ML-TMD and dilute magnetic semiconductor for chiral light emission (top) and out-of-plane magnetic field dependent EL helicity (bottom). Adapted by permission from Springer Nature Customer Service Centre GmbH: Nature Nanotechnology [73] © 2016.

far very few works that couple the valley physics with thermoelectrics. For example, valley-Seebeck effect and valley-Nernst effect have been predicted theoretically in TMDs, zigzag graphene nanoribbons and group-IV MLs [193–195]. An obstacle to the experimental observation of valley Nernst effect is applying the macroscopic temperature gradients in TMDs. However, Dau *et al* have recently grown large area TMD MLs and applied temperature gradients in WSe$_2$ on mm scale [196]. In order to lift the K^+–K^- valley degeneracy, they grow NiFe film on top of the WSe$_2$ layer. By using the FM resonance-spin pumping, spin can be pumped into WSe$_2$ and result in a population imbalance between the two valleys of WSe$_2$. Eventually, the combination of a temperature gradient and valley polarization allows them to successfully detect

valley Nernst effect in WSe$_2$ at room temperature. There is no doubt that these intriguing valleytronic devices could pave the way for future information processing and logic circuits.

6. Challenges and outlook

In this review, we have summarized different strategies for valley modulation in ML TMDs and their hybrid heterostructures. It is seen that, in the past decade, bountiful technologies have been developed to drive the valley degree of freedom in varies of TMD systems to create electronic or optical states with emerging physical phenomena, that may lead to future applications. In spite of the rapid progress in the field of valley manipulation, challenges still remain in a number of aspects.

Firstly, it is crucial, yet not fully understood, to optimize the valleytronic parameters such as valley lifetimes and degree of valley polarization at room temperature. For example, it is by far still an extremely challenging question in modulating the valley polarization of ML-TMDs. Nevertheless, mixing multiple external fields, along with plasmonic architectures, moiré patterns and defects engineering may be considered as one solution to overcome the low degree of valley polarization and short valley lifetimes. In particular, the way to accelerate the valley polarized exciton recombination time and suppress the intervalley scattering is one of the key topics for further investigations.

Secondly, since most of the reported valley photonic and optoelectronic applications are based on exfoliated ML TMDs, the realization of valleytronic devices integrated by ML-TMDs grown by heteroepitaxy or homoepitaxy in a large scale is still missing. However, defects in grown films are known to show strong variations on the optical and/or electrical responses from samples to samples. Deeper understanding on the physical mechanisms of valley depolarization and decoherence influenced by disorders, phonons, defects, etc is largely desired for the realization of large degree of valley polarization at room temperature. On the other hand, although theories have predicted that valley polarization can be realized and tuned in magnetically doped TMDs and ferrovalley materials such as VSe$_2$ [197–199] without external magnetic field or FM substrates, it is highly desired to address the feasibility, applicability, and stability in the future.

As mentioned in the main text of this review, devices taking advantages of the valley degree of freedom, such as valley valve, valley diodes, valley Hall electronics, etc. Additionally, thanks to the open surfaces and jointable edges of TMD materials, those systems are of great promises to show novel physical properties while stacked up vertically or stitched in-plane. Moreover, engineering the interface between ML-TMDs and other functional materials with ferroelectricity and piezoelectricity would give rise to novel valleytronic properties. In general, the investigation of TMD materials and their hybrid heterostructures is opening up new possibilities, which could effectively enhance the functionality of future spin-valleytronic devices, including valley current filters, valley qubits, valley-current amplifiers, non-volatile optical memory, and quantum computation devices in information processing and sensing.

ORCID iDs

Xiaoxi Li ⓘ https://orcid.org/0000-0002-2153-5608
Hanwen Wang ⓘ https://orcid.org/0000-0003-2212-6205
Zheng Han ⓘ https://orcid.org/0000-0001-5721-6206

References

[1] Shimazaki Y, Yamamoto M, Borzenets I V, Watanabe K, Taniguchi T and Tarucha S 2015 Generation and detection of pure valley current by electrically induced Berry curvature in bilayer graphene *Nat. Phys.* **11** 1032–6

[2] Pei F, Laird E A, Steele G A and Kouwenhoven L P 2012 Valley-spin blockade and spin resonance in carbon nanotubes *Nat. Nanotechnol.* **7** 630–4

[3] Goswami S *et al* 2007 Controllable valley splitting in silicon quantum devices *Nat. Phys.* **3** 41–5

[4] Zhang T T, Barate P, Nguyen C T 2013 L-valley electron spin dynamics in GaAs *Phys. Rev.* B **87** 041201

[5] Isberg J, Gabrysch M, Hammersberg J, Majdi S, Kovi K K and Twitchen D J 2013 Generation, transport and detection of valley-polarized electrons in diamond *Nat. Mater.* **12** 760–4

[6] Xiao D, Yao W and Niu Q 2007 Valley-contrasting physics in graphene: magnetic moment and topological transport *Phys. Rev. Lett.* **99** 236809

[7] Rycerz A, Tworzydło J and Beenakker C W J 2007 Valley filter and valley valve in graphene *Nat. Phys.* **3** 172–5

[8] Mak K F, He K, Shan J and Heinz T F 2012 Control of valley polarization in monolayer MoS$_2$ by optical helicity *Nat. Nanotechnol.* **7** 494–8

[9] Mak K F, Xiao D and Shan J 2018 Light-valley interactions in 2D semiconductors *Nat. Photon.* **12** 451–60

[10] Schaibley J R *et al* 2016 Valleytronics in 2D materials *Nat. Rev. Mater.* **1** 16055

[11] Xu X, Yao W, Xiao D and Heinz T F 2014 Spin and pseudospins in layered transition metal dichalcogenides *Nat. Phys.* **10** 343–50

[12] Wang G *et al* 2016 Control of exciton valley coherence in transition metal dichalcogenide monolayers *Phys. Rev. Lett.* **117** 187401

[13] Ye Z, Sun D and Heinz T F 2017 Optical manipulation of valley pseudospin *Nat. Phys.* **13** 26–9

[14] Hao K *et al* 2016 Direct measurement of exciton valley coherence in monolayer WSe$_2$ *Nat. Phys.* **12** 677–82

[15] Cao T *et al* 2012 Valley-selective circular dichroism of monolayer molybdenum disulphide *Nat. Commun.* **3** 887

[16] Zeng H, Dai J, Yao W, Xiao D and Cui X 2012 Valley polarization in MoS$_2$ monolayers by optical pumping *Nat. Nanotechnol.* **7** 490–3

[17] Wang Z, Chiu Y-H, Honz K, Mak K F and Shan J 2018 Electrical tuning of interlayer exciton gases in WSe$_2$ bilayers *Nano Lett.* **18** 137–43

[18] Wu S *et al* 2013 Electrical tuning of valley magnetic moment through symmetry control in bilayer MoS$_2$ *Nat. Phys.* **9** 149–53

[19] Lee J, Mak K F and Shan J 2016 Electrical control of the valley Hall effect in bilayer MoS$_2$ transistors *Nat. Nanotechnol.* **11** 421–5

[20] Liu F, Zhou J, Zhu C and Liu Z 2017 Electric field effect in two-dimensional transition metal dichalcogenides *Adv. Funct. Mater.* **27** 1602404

[21] Aivazian G *et al* 2015 Magnetic control of valley pseudospin in monolayer WSe$_2$ *Nat. Phys.* **11** 148–52

[22] Smolenski T, Goryca M, Koperski M 2016 Tuning valley polarization in a WSe$_2$ monolayer with a tiny magnetic field *Phys. Rev.* X **6** 021024

[23] Shinokita K, Wang X, Miyauchi Y, Watanabe K, Taniguchi T and Matsuda K 2019 Continuous control and enhancement of excitonic valley polarization in monolayer WSe$_2$ by electrostatic doping *Adv. Funct. Mater.* **29** 1900260

[24] Lorchat E, Azzini S, Chervy T, Taniguchi T, Watanabe K, Ebbesen T W, Genet C and Berciaud S 2018 Room-temperature valley polarization and coherence in transition metal dichalcogenide-graphene van der Waals heterostructures *ACS Photon.* **5** 5047–54

[25] Wan Y *et al* 2018 Epitaxial single-layer MoS$_2$ on GaN with enhanced valley helicity *Adv. Mater.* **30** 1703888

[26] Lin W-H, Tseng W-S, Went C M, Marcus L T, George R R, Harry A A and Nai-Chang Y 2019 Nearly 90% circularly polarized emission in monolayer WS$_2$ single crystals by chemical vapor deposition *ACS Nano* **14** 1350–9

[27] McCreary K M, Currie M, Hanbicki A T, Chuang H-J and Jonker B T 2017 Understanding variations in circularly polarized photoluminescence in monolayer transition metal dichalcogenides *ACS Nano* **11** 7988–94

[28] Zhao C *et al* 2017 Enhanced valley splitting in monolayer WSe$_2$ due to magnetic exchange field *Nat. Nanotechnol.* **12** 757–62

[29] Norden T *et al* 2019 Giant valley splitting in monolayer WS$_2$ by magnetic proximity effect *Nat. Commun.* **10** 4163

[30] Jin C *et al* 2018 Imaging of pure spin-valley diffusion current in WS$_2$–WSe$_2$ heterostructures *Science* **360** 893–6

[31] Jiang C *et al* 2018 Microsecond dark-exciton valley polarization memory in two-dimensional heterostructures *Nat. Commun.* **9** 753

[32] Li Z *et al* 2018 Tailoring MoS$_2$ valley-polarized photoluminescence with super chiral near-field *Adv. Mater.* **30** 1801908

[33] Gong S-H, Alpeggiani F, Sciacca B, Garnett E C and Kuipers L 2018 Nanoscale chiral valley-photon interface through optical spin–orbit coupling *Science* **359** 443–7

[34] Xiao D *et al* 2012 Coupled spin and valley physics in monolayers of MoS$_2$ and other group-VI dichalcogenides *Phys. Rev. Lett.* **108** 196802

[35] Vitale S A, Nezich D, Varghese J O, Kim P, Gedik N, Jarillo-Herrero P, Xiao D and Rothschild M 2018 Valleytronics: opportunities, challenges, and paths forward *Small* **14** 1801483

[36] Wang G *et al* 2017 In-plane propagation of light in transition metal dichalcogenide monolayers: optical selection rules *Phys. Rev. Lett.* **119** 047401

[37] Taniyama T, Wada E, Itoh M and Yamaguchi M 2011 Electrical and optical spin injection in ferromagnet/semiconductor heterostructures *NPG Asia Mater.* **3** 65–73

[38] Mak K F, McGill K L, Park J and McEuen P L 2014 The valley Hall effect in MoS$_2$ transistors *Science* **344** 1489–92

[39] Ubrig N, Jo S, Philippi M, Costanzo D, Berger H, Kuzmenko A B and Morpurgo A F 2017 Microscopic origin of the valley Hall effect in transition metal dichalcogenides revealed by wavelength-dependent mapping *Nano Lett.* **17** 5719–25

[40] Safeer C K *et al* 2019 Room-temperature spin Hall effect in graphene/MoS$_2$ van der Waals heterostructures *Nano Lett.* **19** 1074–82

[41] Feng W, Yao Y, Zhu W 2012 Intrinsic spin Hall effect in monolayers of group-VI dichalcogenides: a first-principles study *Phys. Rev.* B **86** 165108

[42] Tahir M, Manchon A and Schwingenschloegl U 2014 Photoinduced quantum spin and valley Hall effects, and orbital magnetization in monolayer MoS$_2$ *Phys. Rev.* B **90** 125438

[43] Wu G Y and Lue N Y 2012 Graphene-based qubits in quantum communications *Phys. Rev.* B **86** 045456

[44] Lee M K, Lue N Y, Wen C K 2012 Valley-based field-effect transistors in graphene *Phys. Rev.* B **86** 165411

[45] Wang Y, Cong C, Shang J, Eginligil M, Jin Y, Li G, Chen Y, Peimyoo N and Yu T 2019 Unveiling exceptionally robust valley contrast in AA- and AB-stacked bilayer WS$_2$ *Nanoscale Horiz.* **4** 396–403

[46] Yu T and Wu M W 2016 Valley depolarization dynamics and valley Hall effect of excitons in monolayer and bilayer MoS$_2$ *Phys. Rev.* B **93** 045414

[47] Zhu B, Zeng H, Dai J, Gong Z and Cui X 2014 Anomalously robust valley polarization and valley coherence in bilayer WS$_2$ *Proc. Natl Acad. Sci. USA* **111** 11606–11

[48] Su H, Wei C, Deng A, Deng D, Yang C and Dai J-F 2017 Anomalous enhancement of valley polarization in multilayer WS$_2$ at room temperature *Nanoscale* **9** 5148–54

[49] Godiksen R H *et al* 2020 Contrast in spin-valley polarization due to competing indirect transitions in few-layer WS$_2$ and WSe$_2$ (arXiv:2006.01970)

[50] Ramasubramaniam A 2012 Large excitonic effects in monolayers of molybdenum and tungsten dichalcogenides *Phys. Rev.* B **86** 115409

[51] Robert C *et al* 2016 Exciton radiative lifetime in transition metal dichalcogenide monolayers *Phys. Rev.* B **93** 205423

[52] Wang L and Wu M W 2014 Electron spin relaxation due to D'yakonov–Perel' and Elliot–Yafet mechanisms in monolayer MoS$_2$: role of intravalley and intervalley processes *Phys. Rev.* B **89** 115302

[53] Yu T and Wu M W 2014 Valley depolarization due to intervalley and intravalley electron–hole exchange interactions in monolayer MoS$_2$ *Phys. Rev.* B **89** 205303

[54] Glazov M M *et al* 2014 Exciton fine structure and spin decoherence in monolayers of transition metal dichalcogenides *Phys. Rev.* B **89** 201302

[55] Wang G, Bouet L, Lagarde D 2014 Valley dynamics probed through charged and neutral exciton emission in monolayer WSe$_2$ *Phys. Rev.* B **90** 075413

[56] Jakubczyk T, Delmonte V, Koperski M, Nogajewski K, Faugeras C, Langbein W, Potemski M and Kasprzak J 2016 Radiatively limited dephasing and exciton dynamics in MoSe$_2$ monolayers revealed with four-wave mixing microscopy *Nano Lett.* **16** 5333–9

[57] Zhu C R *et al* 2014 Exciton valley dynamics probed by Kerr rotation in WSe$_2$ monolayers *Phys. Rev.* B **90** 161302

[58] Zhang X-X *et al* 2017 Magnetic brightening and control of dark excitons in monolayer WSe$_2$ *Nat. Nanotechnol.* **12** 883–8

[59] Tang Y, Mak K F and Shan J 2019 Long valley lifetime of dark excitons in single-layer WSe$_2$ *Nat. Commun.* **10** 4047

[60] McCormick E J, Newburger M J, Luo Y K, McCreary K M, Singh S, Martin I B, Cichewicz E J, Jonker B T and Kawakami R K 2018 Imaging spin dynamics in monolayer WS$_2$ by time-resolved Kerr rotation microscopy *2D Mater.* **5** 011010

[61] Rivera P, Seyler K L, Yu H, Schaibley J R, Yan J, Mandrus D G, Yao W and Xu X 2016 Valley-polarized exciton dynamics in a 2D semiconductor heterostructure *Science* **351** 688–91

[62] Rivera P *et al* 2015 Observation of long-lived interlayer excitons in monolayer MoSe$_2$–WSe$_2$ heterostructures *Nat. Commun.* **6** 1–6

[63] Hsu W-T *et al* 2015 Optically initialized robust valley-polarized holes in monolayer WSe$_2$ *Nat. Commun.* **6** 1–8

[64] Kim J *et al* 2017 Observation of ultralong valley lifetime in WSe$_2$/MoS$_2$ heterostructures *Sci. Adv.* **3** e1700518

[65] Dey P *et al* 2017 Gate-controlled spin-valley locking of resident carriers in WSe$_2$ monolayers *Phys. Rev. Lett.* **119** 137401

[66] Kha T *et al* 2017 Disorder-dependent valley properties in monolayer WSe$_2$ *Phys. Rev.* B **96** 041302

[67] Neumann A, Lindlau J, Colombier L, Nutz M, Najmaei S, Lou J, Mohite A D, Yamaguchi H and Högele A 2017 Opto-valleytronic imaging of atomically thin semiconductors *Nat. Nanotechnol.* **12** 329–34

[68] Moody G *et al* 2018 Microsecond valley lifetime of defect-bound excitons in monolayer WSe$_2$ *Phys. Rev. Lett.* **121** 057403

[69] He Y-M *et al* 2015 Single quantum emitters in monolayer semiconductors *Nat. Nanotechnol.* **10** 497–502

[70] Koperski M, Nogajewski K, Arora A, Cherkez V, Mallet P, Veuillen J-Y, Marcus J, Kossacki P and Potemski M 2015 Single photon emitters in exfoliated WSe$_2$ structures *Nat. Nanotechnol.* **10** 503–6

[71] Chakraborty C, Kinnischtzke L, Goodfellow K M, Beams R and Vamivakas A N 2015 Voltage-controlled quantum light from an atomically thin semiconductor *Nat. Nanotechnol.* **10** 507–11

[72] Wang Z, Rhodes D A, Watanabe K, Taniguchi T, Hone J C, Shan J and Mak K F 2019 Evidence of high-temperature exciton condensation in two-dimensional atomic double layers *Nature* **574** 76–80

[73] Ye Y *et al* 2016 Electrical generation and control of the valley carriers in a monolayer transition metal dichalcogenide *Nat. Nanotechnol.* **11** 597–602

[74] Yang L, Sinitsyn N A, Chen W, Yuan J, Zhang J, Lou J and Crooker S A 2015 Long-lived nanosecond spin relaxation and spin coherence of electrons in monolayer MoS$_2$ and WS$_2$ *Nat. Phys.* **11** 830–4

[75] Mai C, Barrette A, Yu Y, Semenov Y G, Kim K W, Cao L and Gundogdu K 2014 Many-body effects in valleytronics: direct measurement of valley lifetimes in single-layer MoS$_2$ *Nano Lett.* **14** 202–6

[76] Sallen G, Bouet L, Marie X 2012 Robust optical emission polarization in MoS$_2$ monolayers through selective valley excitation *Phys. Rev.* B **86** 081301

[77] Sie E J, McIver J W, Lee Y-H, Fu L, Kong J and Gedik N 2015 Valley-selective optical Stark effect in monolayer WS$_2$ *Nat. Mater.* **14** 290–4

[78] LaMountain T, Bergeron H, Balla I 2018 Valley-selective optical Stark effect probed by Kerr rotation *Phys. Rev.* B **97** 045307

[79] Kim J, Hong X, Jin C, Shi S-F, Chang C-Y S, Chiu M-H, Li L-J and Wang F 2014 Ultrafast generation of pseudo-magnetic field for valley excitons in WSe$_2$ monolayers *Science* **346** 1205–8

[80] Srivastava A, Sidler M, Allain A V, Lembke D S, Kis A and Imamoğlu A 2015 Valley Zeeman effect in elementary optical excitations of monolayer WSe$_2$ *Nat. Phys.* **11** 141–7

[81] Plechinger G *et al* 2016 Excitonic valley effects in monolayer WS$_2$ under high magnetic fields *Nano Lett.* **16** 7899–904

[82] MacNeill D *et al* 2015 Breaking of valley degeneracy by magnetic field in monolayer MoSe$_2$ *Phys. Rev. Lett.* **114** 037401

[83] Stier A V *et al* 2016 Exciton diamagnetic shifts and valley Zeeman effects in monolayer WS_2 and MoS_2 to 65 Tesla *Nat. Commun.* **7** 10643

[84] Van der Donck M, Zarenia M and Peeters F M 2018 Strong valley Zeeman effect of dark excitons in monolayer transition metal dichalcogenides in a tilted magnetic field *Phys. Rev.* B **97** 081109

[85] Rostami H, Moghaddam A G and Asgari R 2013 Effective lattice Hamiltonian for monolayer MoS_2: tailoring electronic structure with perpendicular electric and magnetic fields *Phys. Rev.* B **88** 085440

[86] Cai T, Yang S A, Li X 2013 Magnetic control of the valley degree of freedom of massive Dirac fermions with application to transition metal dichalcogenides *Phys. Rev.* B **88** 115140

[87] Rose F, Goerbig M O and Piechon F 2013 Spin- and valley-dependent magneto-optical properties of MoS_2 *Phys. Rev.* B **88** 125438

[88] Chu R-L *et al* 2014 Valley-splitting and valley-dependent inter-Landau-level optical transitions in monolayer MoS_2 quantum Hall systems *Phys. Rev.* B **90** 045427

[89] Dal Conte S, Bottegoni F, Pogna E A A 2015 Ultrafast valley relaxation dynamics in monolayer MoS_2 probed by nonequilibrium optical techniques *Phys. Rev.* B **92** 235425

[90] Konabe S 2016 Screening effects due to carrier doping on valley relaxation in transition metal dichalcogenide monolayers *Appl. Phys. Lett.* **109** 073104

[91] Plechinger G, Nagler P, Kraus J, Paradiso N, Strunk C, Schüller C and Korn T 2015 Identification of excitons, trions and biexcitons in single-layer WS_2 *Phys. Status Solidi RRL* **9** 457–61

[92] Hanbicki A T, McCreary K M, Kioseoglou G, Currie M, Hellberg C S, Friedman A L and Jonker B T 2016 High room temperature optical polarization due to spin-valley coupling in monolayer WS_2 *AIP Adv.* **6** 055804

[93] Jones A M *et al* 2013 Optical generation of excitonic valley coherence in monolayer WSe_2 *Nat. Nanotechnol.* **8** 634–8

[94] Miller B *et al* 2019 Tuning the Frohlich exciton–phonon scattering in monolayer MoS_2 *Nat. Commun.* **10** 807

[95] Feng S *et al* 2019 Engineering valley polarization of monolayer WS_2: a physical doping approach *Small* **15** 1805503

[96] Fröhlich H 1954 Electrons in lattice fields *Adv. Phys.* **3** 325–61

[97] Jeong H Y, Jin Y, Yun S J, Zhao J, Baik J, Keum D H, Lee H S and Lee Y H 2017 Heterogeneous defect domains in single-crystalline hexagonal WS_2 *Adv. Mater.* **29** 1605043

[98] Hue L T, Yun S J, Huy T Q and Zhao J 2017 Edge delamination of monolayer transition metal dichalcogenides *ACS Nano* **11** 7534–41

[99] Lin Y-C, Li S, Komsa H-P, Chang L-J, Krasheninnikov A V, Eda G and Suenaga K 2018 Revealing the atomic defects of WS_2 governing its distinct optical emissions *Adv. Funct. Mater.* **28** 1704210

[100] Sheng Y *et al* 2017 Photoluminescence segmentation within individual hexagonal monolayer tungsten disulfide domains grown by chemical vapor deposition *ACS Appl. Mater. Interfaces* **9** 15005–14

[101] Refaely-Abramson S *et al* 2018 Defect-induced modification of low-lying excitons and valley selectivity in monolayer transition metal dichalcogenides *Phys. Rev. Lett.* **121** 167402

[102] Zhang S *et al* 2017 Defect structure of localized excitons in a WSe_2 monolayer *Phys. Rev. Lett.* **119** 046101

[103] Zhu C R, Wang G, Liu B L 2013 Strain tuning of optical emission energy and polarization in monolayer and bilayer MoS_2 *Phys. Rev.* B **88** 121301

[104] Elliott R J 1957 Intensity of optical absorption by excitons *Phys. Rev.* **108** 1384–9

[105] Xu L, Yang M, Shen L 2018 Large valley splitting in monolayer WS_2 by proximity coupling to an insulating antiferromagnetic substrate *Phys. Rev.* B **97** 041405

[106] Zhang Q, Yang S A, Mi W, Cheng Y and Schwingenschlögl U 2016 Large spin-valley polarization in monolayer $MoTe_2$ on top of EuO(111) *Adv. Mater.* **28** 959–66

[107] Peng B *et al* 2017 Valley polarization of trions and magnetoresistance in heterostructures of MoS_2 and yttrium iron garnet *ACS Nano* **11** 12257–65

[108] Zhong D *et al* 2017 Van der Waals engineering of ferromagnetic semiconductor heterostructures for spin and valleytronics *Sci. Adv.* **3** e1603113

[109] Gong C *et al* 2017 Discovery of intrinsic ferromagnetism in two-dimensional van der Waals crystals *Nature* **546** 265–9

[110] Fei Z *et al* 2018 Two-dimensional itinerant ferromagnetism in atomically thin Fe_3GeTe_2 *Nat. Mater.* **17** 778–82

[111] Huang B *et al* 2017 Layer-dependent ferromagnetism in a van der Waals crystal down to the monolayer limit *Nature* **546** 270–3

[112] Burch K S, Mandrus D and Park J-G 2018 Magnetism in two-dimensional van der Waals materials *Nature* **563** 47–52

[113] Bonilla M *et al* 2018 Strong room-temperature ferromagnetism in VSe_2 monolayers on van der Waals substrates *Nat. Nanotechnol.* **13** 289–93

[114] Deng Y *et al* 2018 Gate-tunable room-temperature ferromagnetism in two-dimensional Fe_3GeTe_2 *Nature* **563** 94–9

[115] Huang B *et al* 2018 Electrical control of 2D magnetism in bilayer CrI_3 *Nat. Nanotechnol.* **13** 544–8

[116] Tan C *et al* 2018 Hard magnetic properties in nanoflake van der Waals Fe_3GeTe_2 *Nat. Commun.* **9** 1554

[117] Jiang S, Li L, Wang Z, Mak K F and Shan J 2018 Controlling magnetism in 2D CrI_3 by electrostatic doping *Nat. Nanotechnol.* **13** 549–53

[118] Seyler K L *et al* 2018 Valley manipulation by optically tuning the magnetic proximity effect in WSe_2/CrI_3 heterostructures *Nano Lett.* **18** 3823–8

[119] Cerjan B, Yang X, Nordlander P and Halas N J 2016 Asymmetric aluminium antennas for self-calibrating surface-enhanced infrared absorption spectroscopy *ACS Photon.* **3** 354–60

[120] Murray W A and Barnes W L 2007 Plasmonic materials *Adv. Mater.* **19** 3771–82

[121] Giannini V, Fernández-Domínguez A I, Sonnefraud Y, Roschuk T, Fernández-García R and Maier S A 2010 Controlling light localization and light–matter interactions with nanoplasmonics *Small* **6** 2498–507

[122] Tang Y and Cohen A E 2011 Enhanced enantioselectivity in excitation of chiral molecules by superchiral light *Science* **332** 333–6

[123] Hendry E *et al* 2010 Ultrasensitive detection and characterization of biomolecules using superchiral fields *Nat. Nanotechnol.* **5** 783–7

[124] Govorov A O, Fan Z, Hernandez P, Slocik J M and Naik R R 2010 Theory of circular dichroism of nanomaterials comprising chiral molecules and nanocrystals: plasmon enhancement, dipole interactions, and dielectric effects *Nano Lett.* **10** 1374–82

[125] Kleemann M-E *et al* 2017 Strong-coupling of WSe_2 in ultracompact plasmonic nanocavities at room temperature *Nat. Commun.* **8** 1296

[126] Johnson A D, Cheng F, Tsai Y and Shih C-K 2017 Giant enhancement of defect-bound exciton luminescence and suppression of band-edge luminescence in monolayer WSe_2-Ag plasmonic hybrid structures *Nano Lett.* **17** 4317–22

[127] Cotrufo M, Sun L, Choi J, Alù A and Li X 2019 Enhancing functionalities of atomically thin semiconductors with plasmonic nanostructures *Nanophotonics* **8** 577–98

[128] Wen J *et al* 2017 Room-temperature strong light–matter interaction with active control in single plasmonic nanorod coupled with two-dimensional atomic crystals *Nano Lett.* **17** 4689–97

[129] Dibos A M *et al* 2019 Electrically tunable exciton–plasmon coupling in a WSe_2 monolayer embedded in a plasmonic crystal cavity *Nano Lett.* **19** 3543–7

[130] Li Y, Li Z, Chi C, Shan H, Zheng L and Fang Z 2017 Plasmonics of 2D nanomaterials: properties and applications *Adv. Sci.* **4** 1600430

[131] Ding B, Zhang Z, Chen Y-H, Zhang Y, Blaikie R J and Qiu M 2019 Tunable valley polarized plasmon–exciton polaritons in two-dimensional semiconductors *ACS Nano* **13** 1333–41

[132] Liu W, Lee B, Naylor C H, Ee H-S, Park J, Johnson A T C and Agarwal R 2016 Strong exciton–plasmon coupling in MoS_2 coupled with plasmonic lattice *Nano Lett.* **16** 1262–9

[133] Wu Z, Li J, Zhang X, Redwing J M and Zheng Y 2019 Room-temperature active modulation of valley dynamics in a monolayer semiconductor through chiral Purcell effects *Adv. Mater.* **31** 1904132

[134] Li L *et al* 2020 Room-temperature valleytronic transistor *Nat. Nanotechnol.* **15** 743–9

[135] Yu H, Liu G-B, Tang J, Xu X and Yao W 2017 Moiré excitons: from programmable quantum emitter arrays to spin-orbit-coupled artificial lattices *Sci. Adv.* **3** e1701696

[136] Cao Y, Fatemi V, Fang S, Watanabe K, Taniguchi T, Kaxiras E and Jarillo-Herrero P 2018 Unconventional superconductivity in magic-angle graphene superlattices *Nature* **556** 43–50

[137] Chen G *et al* 2019 Signatures of tunable superconductivity in a trilayer graphene moiré superlattice *Nature* **572** 215–9

[138] Yankowitz M, Chen S, Polshyn H, Zhang Y, Watanabe K, Taniguchi T, Graf D, Young A F and Dean C R 2019 Tuning superconductivity in twisted bilayer graphene *Science* **363** 1059–64

[139] Po H C, Zou L, Vishwanath A 2018 Origin of mott insulating behavior and superconductivity in twisted bilayer graphene *Phys. Rev.* X **8** 031089

[140] Jin C *et al* 2019 Observation of moiré excitons in WSe_2/WS_2 heterostructure superlattices *Nature* **567** 76–80

[141] Alexeev E M *et al* 2019 Resonantly hybridized excitons in moiré superlattices in van der Waals heterostructures *Nature* **567** 81–6

[142] Kha T *et al* 2019 Evidence for moire excitons in van der Waals heterostructures *Nature* **567** 71–5

[143] Seyler K L, Rivera P, Yu H, Wilson N P, Ray E L, Mandrus D G, Yan J, Yao W and Xu X 2019 Signatures of moiré-trapped valley excitons in $MoSe_2$/WSe_2 heterobilayers *Nature* **567** 66–70

[144] Jauregui L A *et al* 2019 Electrical control of interlayer exciton dynamics in atomically thin heterostructures *Science* **366** 870–5

[145] Kunstmann J *et al* 2018 Momentum-space indirect interlayer excitons in transition-metal dichalcogenide van der Waals heterostructures *Nat. Phys.* **14** 801–5

[146] Nagler P *et al* 2017 Giant magnetic splitting inducing near-unity valley polarization in van der Waals heterostructures *Nat. Commun.* **8** 1551

[147] Jin C *et al* 2019 Identification of spin, valley and moiré quasi-angular momentum of interlayer excitons *Nat. Phys.* **15** 1140–4

[148] Lagarde D *et al* 2014 Carrier and polarization dynamics in monolayer MoS_2 *Phys. Rev. Lett.* **112** 047401

[149] Chervy T, Azzini S, Lorchat E, Wang S, Gorodetski Y, Hutchison J A, Berciaud S, Ebbesen T W and Genet C 2018 Room temperature chiral coupling of valley excitons with spin-momentum locked surface plasmons *ACS Photon.* **5** 1281–7

[150] Ciarrocchi A, Unuchek D, Avsar A, Watanabe K, Taniguchi T and Kis A 2019 Polarization switching and electrical control of interlayer excitons in two-dimensional van der Waals heterostructures *Nat. Photon.* **13** 131–6

[151] Hanbicki A T, Chuang H-J, Rosenberger M R, Hellberg C S, Sivaram S V, McCreary K M, Mazin I I and Jonker B T 2018 Double indirect interlayer exciton in a $MoSe_2$/WSe_2 van der Waals heterostructure *ACS Nano* **12** 4719–26

[152] Sun L *et al* 2019 Separation of valley excitons in a MoS_2 monolayer using a subwavelength asymmetric groove array *Nat. Photon.* **13** 180–4

[153] Unuchek D, Ciarrocchi A, Avsar A, Sun Z, Watanabe K, Taniguchi T and Kis A 2019 Valley-polarized exciton currents in a van der Waals heterostructure *Nat. Nanotechnol.* **14** 1104–9

[154] Gant P, Huang P, Pérez de Lara D, Guo D, Frisenda R and Castellanos-Gomez A 2019 A strain tunable single-layer MoS_2 photodetector *Mater. Today* **27** 8–13

[155] Liao W, Huang Y, Wang H and Zhang H 2019 Van der Waals heterostructures for optoelectronics: progress and prospects *Appl. Mater. Today* **16** 435–55

[156] Qiao H *et al* 2020 Black phosphorous photodetectors *Black Phosphorus* (Berlin: Springer) pp 171–86

[157] Chen X *et al* 2017 Widely tunable black phosphorus mid-infrared photodetector *Nat. Commun.* **8** 1672

[158] Huang L *et al* 2018 Waveguide-integrated black phosphorus photodetector for mid-infrared applications *ACS Nano* **13** 913–21

[159] Li A *et al* 2019 Photodetectors: ultrahigh-sensitive broad-band photodetectors based on dielectric shielded $MoTe_2$/graphene/SnS_2 p–g–n junctions (Adv. Mater. 6/2019) *Adv. Mater.* **31** 1970040

[160] Zhao S, Wu J, Jin K, Ding H, Li T, Wu C, Pan N and Wang X 2018 Highly polarized and fast photoresponse of black phosphorus-InSe vertical p–n heterojunctions *Adv. Funct. Mater.* **28** 1802011

[161] Yuan H *et al* 2014 Generation and electric control of spin-valley-coupled circular photogalvanic current in WSe_2 *Nat. Nanotechnol.* **9** 851–7

[162] Yan W *et al* 2016 A two-dimensional spin field-effect switch *Nat. Commun.* **7** 13372

[163] Eginligil M *et al* 2015 Dichroic spin-valley photocurrent in monolayer molybdenum disulphide *Nat. Commun.* **6** 7636

[164] Dankert A and Dash S P 2017 Electrical gate control of spin current in van der Waals heterostructures at room temperature *Nat. Commun.* **8** 16093

[165] Benítez L A A, Savero Torres W, Sierra J F, Timmermans M, Garcia J H, Roche S, Costache M V and Valenzuela S O 2020 Tunable room-temperature spin galvanic and spin Hall effects in van der Waals heterostructures *Nat. Mater.* **19** 170–5

[166] Liang S *et al* 2017 Electrical spin injection and detection in molybdenum disulfide multilayer channel *Nat. Commun.* **8** 14947

[167] Omar S and van Wees B J 2017 Graphene-WS_2 heterostructures for tunable spin injection and spin transport *Phys. Rev.* B **95** 081404

[168] Xie L and Cui X 2016 Manipulating spin-polarized photocurrents in 2D transition metal dichalcogenides *Proc. Natl Acad. Sci. USA* **113** 3746–50

[169] Chen X, Yan T, Zhu B, Yang S and Cui X 2017 Optical control of spin polarization in monolayer transition metal dichalcogenides *ACS Nano* **11** 1581–7

[170] Ghiasi T S S, Ingla-Aynés J, Kaverzin A A and van Wees B J 2017 Large proximity-induced spin lifetime anisotropy in transition-metal dichalcogenide/graphene heterostructures *Nano Lett.* **17** 7528–32

[171] Yan W *et al* 2016 Long spin diffusion length in few-layer graphene flakes *Phys. Rev. Lett.* **117** 147201

[172] Kamalakar M V, Groenveld C, Dankert A and Dash S P 2015 Long distance spin communication in chemical vapour deposited graphene *Nat. Commun.* **6** 6766

[173] Gmitra M and Fabian J 2015 Graphene on transition-metal dichalcogenides: a platform for proximity spin–orbit physics and optospintronics *Phys. Rev.* B **92** 155403

[174] Luo Y K K, Xu J, Zhu T, Wu G, McCormick E J, Zhan W, Neupane M R and Kawakami R K 2017 Opto-valleytronic spin injection in monolayer MoS_2/few-layer graphene hybrid spin valves *Nano Lett.* **17** 3877–83

[175] Xia Y *et al* 2009 Observation of a large-gap topological-insulator class with a single Dirac cone on the surface *Nat. Phys.* **5** 398–402

[176] Li C H H, van't Erve O M J, Robinson J T, Liu Y, Li L and Jonker B T 2014 Electrical detection of charge-current-induced spin polarization due to spin-momentum locking in Bi_2Se_3 *Nat. Nanotechnol.* **9** 218–24

[177] Dankert A, Geurs J, Kamalakar M V, Charpentier S and Dash S P 2015 Room temperature electrical detection of spin polarized currents in topological insulators *Nano Lett.* **15** 7976–81

[178] Tian J, Hong S, Miotkowski I, Datta S and Chen Y P 2017 Observation of current-induced, long-lived persistent spin polarization in a topological insulator: a rechargeable spin battery *Sci. Adv.* **3** e1602531

[179] Cha S *et al* 2018 Generation, transport and detection of valley-locked spin photocurrent in WSe_2-graphene-Bi_2Se_3 heterostructures *Nat. Nanotechnol.* **13** 910–4

[180] Zhang X-X *et al* 2019 Zeeman-induced valley-sensitive photocurrent in monolayer MoS_2 *Phys. Rev. Lett.* **122** 127401

[181] Zhang Y J, Oka T, Suzuki R, Ye J T and Iwasa Y 2014 Electrically switchable chiral light-emitting transistor *Science* **344** 725–8

[182] Onga M, Zhang Y, Suzuki R and Iwasa Y 2016 High circular polarization in electroluminescence from $MoSe_2$ *Appl. Phys. Lett.* **108** 073107

[183] Yang W *et al* 2016 Electrically tunable valley-light emitting diode (vLED) based on CVD-grown monolayer WS_2 *Nano Lett.* **16** 1560–7

[184] Dankert A *et al* 2017 Spin-polarized tunneling through chemical vapor deposited multilayer molybdenum disulfide *ACS Nano* **11** 6389–95

[185] Dolui K *et al* 2014 Efficient spin injection and giant magnetoresistance in Fe/MoS_2/Fe junctions *Phys. Rev.* B **90** 041401

[186] Wang W *et al* 2015 Spin-valve effect in NiFe/MoS_2/NiFe junctions *Nano Lett.* **15** 5261–7

[187] Rotjanapittayakul W, Pijitrojana W, Archer T, Sanvito S and Prasongkit J 2018 Spin injection and magnetoresistance in MoS_2-based tunnel junctions using Fe_3Si Heusler alloy electrodes *Sci. Rep.* **8** 4779

[188] Sanchez O L, Ovchinnikov D, Misra S, Allain A and Kis A 2016 valley polarization by spin injection in a light-emitting van der Waals heterojunction *Nano Lett.* **16** 5792–7

[189] Zhai X, Zhang S, Zhao Y, Zhang X and Yang Z 2016 Bipolar spin-valley diode effect in a silicene magnetic junction *Appl. Phys. Lett.* **109** 122404

[190] Zhai X *et al* 2019 Valley-mediated and electrically switched bipolar-unipolar transition of the spin-diode effect in heavy group-IV monolayers *Phys. Rev. Appl.* **11** 064047

[191] Lee J, Wang Z, Xie H, Mak K F and Shan J 2017 Valley magnetoelectricity in single-layer MoS_2 *Nat. Mater.* **16** 887–91

[192] Kim Y and Lee J D 2019 Anomalous electron dynamics induced through the valley magnetic domain: a pathway to valleytronic current processing *Nano Lett.* **19** 4166–73

[193] Konabe S and Yamamoto T 2014 Valley photothermoelectric effects in transition-metal dichalcogenides *Phys. Rev.* B **90** 075430

[194] Yu Z, Xu F and Wang J 2016 Valley Seebeck effect in gate tunable zigzag graphene nanoribbons *Carbon* **99** 451–5

[195] Zhai X, Wang S and Zhang Y 2017 Valley-spin Seebeck effect in heavy group-IV monolayers *New J. Phys.* **19** 063007

[196] Tuan D M *et al* 2019 The valley Nernst effect in WSe_2 *Nat. Commun.* **10** 5796

[197] Yu W *et al* 2019 Chemically exfoliated VSe_2 monolayers with room-temperature ferromagnetism *Adv. Mater.* **31** 1903779

[198] Tong W-Y *et al* 2016 Concepts of ferrovalley material and anomalous valley Hall effect *Nat. Commun.* **7** 13612

[199] Liu J, Hou W-J, Cheng C, Fu H-X, Sun J-T and Meng S 2017 Intrinsic valley polarization of magnetic VSe_2 monolayers *J. Phys.: Condens. Matter* **29** 255501